MODELING AND SIMULATION OF A GRID CONNECTED SOLAR-HYDRO HYBRID SYSTEM TO SUPPLEMENT POWER SUPPLY IN KADUNA NORTH

BY

AMINU JIBRIN

DEPARTMENT OF ELECTRICAL AND COMPUTER ENGINEERING

FACULTY OF ENGINEERING

AHMADU BELLO UNIVERSITY, ZARIA

NIGERIA

NOVEMBER, 2015

MODELING AND SIMULATION OF A GRID CONNECTED SOLAR-HYDRO HYBRID SYSTEM TO SUPPLEMENT POWER SUPPLY IN KADUNA NORTH

BY

AMINU JIBRIN, B.ENG (KUST), 2010

MSC/ENG/3468/2011-2012

A DISSERTATION SUBMITTED TO THE SCHOOL OF POSTGRADUATE STUDIES, AHMADU BELLO UNIVERSITY, ZARIA IN PARTIAL FULFILLMENT OF THE REQUIREMENTS FOR THE AWARD OF MASTER DEGREE IN ELECTRICAL ENGINEERING

DEPARTMENT OF ELECTRICAL AND COMPUTER ENGINEERING

FACULTY OF ENGINEERING

AHMADU BELLO UNIVERSITY, ZARIA

NIGERIA

NOVEMBER, 2015

DECLARATION

I Aminu JIBRIN declare that this dissertation entitled "Development and Simulation of a Grid Connected Solar-Hydro Hybrid System to Supplement Power Supply in Kaduna North" has been carried out by me in the Department of Electrical and Computer Engineering, Ahmadu Bello University Zaria. The information derived from the literature has been duly acknowledged in the text and a list of references provided. No part of this dissertation was previously presented for another degree or diploma at this or any other Institution.

Aminu JIBRIN _____ _____

Signature Date

CERTIFICATION

This dissertation entitled "DEVELOPMENT AND SIMULATION OF A GRID CONNECTED SOLAR-HYDRO HYBRID SYSTEM TO SUPPLEMENT POWER SUPPLY IN KADUNA NORTH" by AMINU JIBRIN meets the regulations governing the award of degree of Master of Science (M.Sc.) in Electrical Engineering of the Ahmadu Bello University, and is approved for its contribution to knowledge and literary presentation.

Prof. B. Jimoh

(Chairman Supervisory Committee) _____ _____

(Signature) Date

Dr. A. A. Mati

(Member Supervisory Committee) _____ _____

(Signature) Date

Dr. Y. Jibril

(Head of Department) _____ _____

(Signature) Date

Prof. K. Bala

(Dean School of Postgraduate Studies) _____ _____

(Signature) Date

DEDICATION

I dedicate this work to God Almighty for His guidance, kindness, mercy and to my parents, family and friends for their support and prayers.

ACKNOWLEDGEMENTS

My profound gratitude to God Almighty for giving me the opportunity and sparing my life and the good health He has bestowed on me during the course of writing this dissertation work.

I wish to extend my appreciation and thanks to my supervisors, Prof. B. Jimoh and Dr. A. A. Mati for their immense contribution, patience and time to see that this work has become a reality, in terms of richness and content.

I wish to extend my sincere appreciation and thanks to my parents Late Alh. J. Abubakar, A. Jibrin and S. Jibrin. My brothers and sisters H. Jibrin, Dr. B. Jibrin, F. Tech. H. Jibrin, Flying Officer A. Jibrin, Engr. F. Jibrin, N. Jibrin, U. F. Jibrin, I. Anchau and M. Ibrahim for their assistance, prayers, sponsorship and support.

To my mentors, Prof. B. J. Bajoga, Prof. U. O. Aliyu, Prof. M. B. Muazu, Dr. S. M. Sani, Dr. Usman, Dr. A. M. S. Tekanyi, I appreciate your effort and I say thank you for your patience and time for going through my manuscript.

I am grateful to all my lecturers; Dr. J. Y. Oricha, Dr S. Garba, Dr. O. Akinsami, Dr. Y. Jibril, Y. S. Abubakar and all those whose names are not captured here for their effort and encouragement throughout the course of this work.

Also I wish to extend my gratitude to my friends, Mr A. S. Adamu, Mr J. Haruna, E. Okafor, I. Yusif, B. O. Sadiq, I. Zubairu, M. Shamwil, A. Abdullahi, A. Abdullahi, U. Abdullahi, U. Muhammad, I. Ismail, K. Ismail, U. F. Zubair, F. Malali and K. Abubakar for their advices, encouragement, understanding and kind assistance.

Aminu JIBRIN

November, 2015

ABSTRACT

The increasing and stochastic nature of consumers' demand on electricity brought about the need for alternative means of complimenting the existing energy demand. In this research work, a grid connected hybrid system was modeled to support and improve the power quantity of the Kaduna north existing network. Load profiling was done using Artificial Neural Network based on Bayesian regularization algorithm to determine one year load demand of the area under study. The load profiling was carried out and deficit power of 3.21MW was obtained which brought the need to augment the power from the grid using solar-hydro hybrid system. The developed hybrid system was interfaced to the grid via a step-up transformer and a phase locked loop was designed to synchronize the hybrid system with the grid. The solar photovoltaic system adopted the use of Solarex MSX64 using average solar radiation intensity of 653.45W/m^2. The photovoltaic array consist of 50 parallel connected strings and each string consist of 80 series connected photovoltaic modules while two hydro turbines that employed the use of 1.5MW reaction turbine coupled with self-excited induction generator were used for hydropower system development. An average head of 6.04m and discharge of 25.6m^3/s were used in design of the hydropower system. The developed hybrid system was implemented on a Matlab/Simulink environment. The output voltage of the solar photovoltaic cell was boosted using boost converter before connection to DC link bus bar while the AC voltage of the hydro system was converted to DC voltage using universal bridge converter before connecting to the DC link Bus bar. An inverter was used to convert the DC voltage of the hybrid system to AC voltage and a step-up power transformer was used to step the voltage to the utility grid voltage. Phase locked loop was designed to enable synchronization of the hybrid system with the grid. Based on the result obtained, the hydropower system produced 2.88MW and the solar photovoltaic system produced 330kW. The hybrid system was able to supplement a total power of 3.21MW to the grid. The developed model result was validated using a standard model results as contained in the work of Meshram *et al* (2013). The hybrid system modeled was able to carter for the deficit power from the grid and also improves the power quality and security of the grid.

TABLE OF CONTENTS

CHAPTER ONE: GENERAL INTRODUCTION

CHAPTER TWO: LITERATURE REVIEW

CHAPTER THREE: MATERIALS AND METHODS

APPENDICES

LIST OF FIGURES

LIST OF TABLES

LIST OF ABBREVIATIONS

Abbreviations	Definition
AGC	Automatic Generation Control
ALC	Adaptive Linear Combiner
ANN	Artificial Neural Networks
HES	Hybrid Electric Renewable
MATLAB	Matrix Laboratory
NIMET	National Meteorological Agency
PHCN	Power Holding Company of Nigeria
PLL	Phase Lock Loop
PV	Photovoltaic
PWM	Pulse Width Modulation
SEIG	Self-Excited Induction Generator
TCN	Transmission Company of Nigeria

CHAPTER ONE

GENERAL INTRODUCTION

1.1 General Background

In order to move towards a sustainable existence in our critically energy dependent society, there is a continuing need to adopt environmentally sustainable methods for energy production. In Nigeria, as in most developing nations, the demand for sustainable energy is increasing due to population and developmental growth (Otun *et al,* 2012). Researches in this field have developed several methods of generating clean and affordable energy. Even though the use of fossil fuels for generation of electrical energy is more than the use of renewable sources, decreasing oil reserves in the world makes the potential for fossil fuels as a future resource of energy to be decreasing (Zehra and Muhsin, 2013). This leads to a significant interest in renewable energy sources therefore, making transition from fossil fuels towards renewable energy unavoidable (Zehra and Muhsin, 2013). The dependency on safe energy production system from renewable energy is increasing and gaining ground with the support from government policy around the world, especially with the instability of oil in the Middle East and the recent Fukushima nuclear disaster (Jungjohann and Rickerson, 2011). Renewable energy technologies offer the promise of clean, abundant energy gathered from self-renewing resources such as the sun, wind, water, earth and plants (Dorin *et al,* 2009). In most cases, one renewable energy system cannot fulfill the power requirement alone as it is intermittent in nature hence the solution is to hybridized the renewable energy systems (Meshram *et al,* 2013). To satisfy the power requirement, integration of the power grid is required. For supplying electric power in areas using this hybrid system, the power grid may be integrated. For the development of a system that will augment deficit of power, load forecasting is necessary.

1.2 Challenges Facing Nigeria Power System

Nigeria power system is facing enormous challenges such as high-energy losses due to the physical deterioration of the transmission and distribution facilities, inadequate metering system, increase in illegal connection, manpower constraints and inadequate support facilities, high cost of electricity production, inadequate basic industries to service the power sector, poor billing system, poor settlements of bills by consumers and low available capacity (Nasir, 2009). These factors are affecting the performance of the power sector both technically and economically.

1.3 Kaduna Sub-Transmission Network

Kaduna sub-transmission network is a network diagram of the injection substations of both the 33kV and 11kV Feeders in Kaduna north. The network comprises of one transmission station (Mando) feeding the five injection substations in Kaduna north. The five injection substations are Kawo injection substation, Dawaki injection substation, Abakpa injection substation, Mogadishu injection substation and Rigasa injection substation. Mando transmission station does not only feed the five injection substations in Kaduna north but also supply power to other substations outside Kaduna. Four out of the five injection substations are being fed by Mando transmission station while the Mogadishu is being fed by both Mando transmission station and 132kV power generation station. Figure 1.1 shows the Kaduna sub-transmission network.

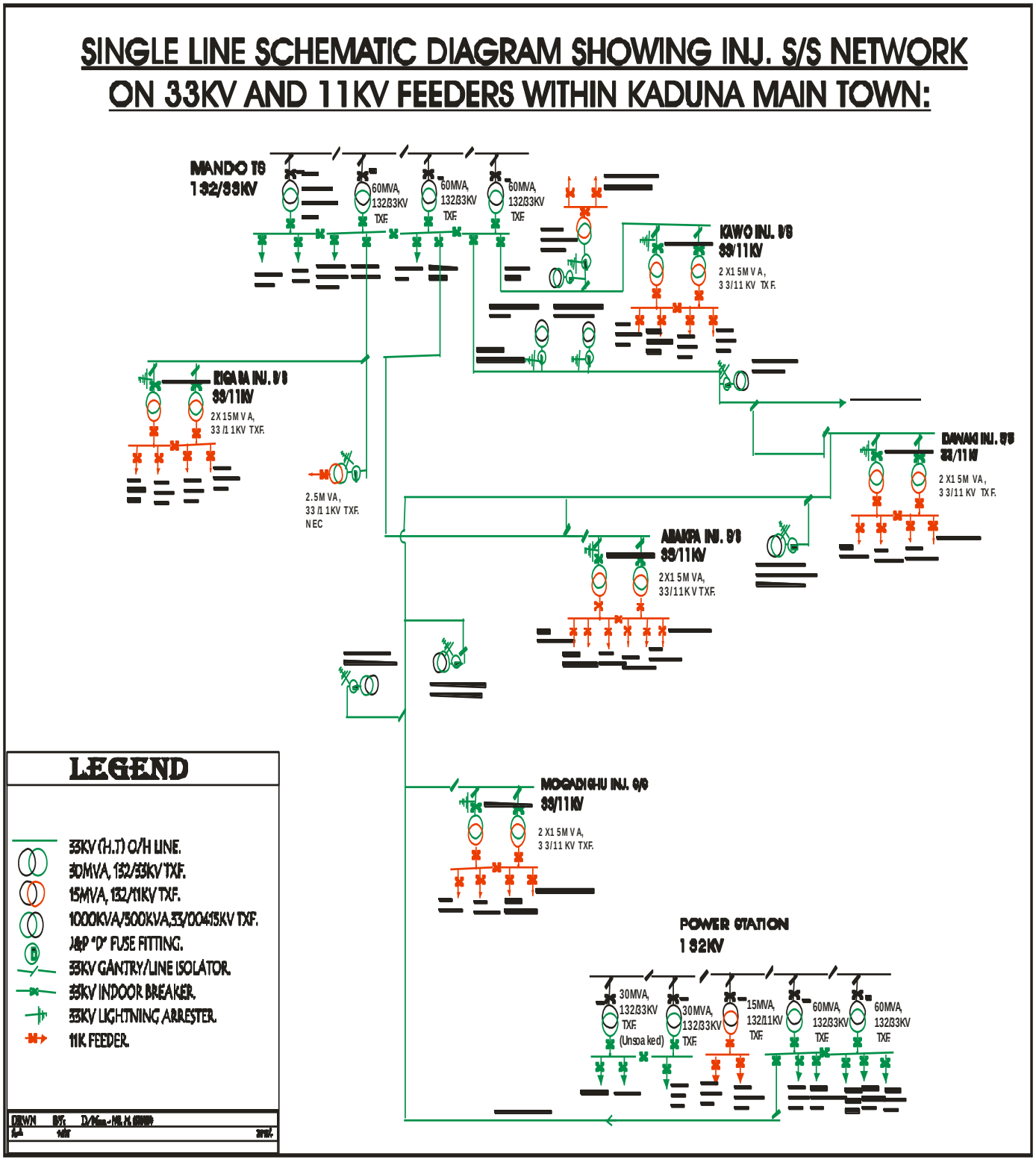

Figure 1.1: Kaduna Sub-Transmission Network (Catalog on Planning and Construction PHCN, 2012)

Dawaki injection substation is one of the most important substations in Kaduna metropolis. This is because it supplies power to many important areas such as Government house, Nigerian television authority (N.T.A) transmission station, liberty radio, independent national electoral commission (INEC) office, national youth service corps (NYSC) secretariat among others.

1.4 Problem Statement

A number of research works had been conducted to augment the deficit of power in the grid which is due to increasing demand of energy and insufficient generation. Power from the grid was not sufficient due to network expansion, urbanization, migration and greater demand of power by the consumers and no plan for increase in generation by the utility was made. This results in load shading by the utility in order to balance the generation with the load. This decreases the power quality and security of the utility grid and brought the need for alternative means of power generation to support the utility grid. In this work, load profiling was done using artificial neural network based on Bayesian regularization algorithm. The model was developed putting in cognizance the effect of environmental condition which includes temperature, relative humidity, rainfall, wind speed, solar radiation and sunshine hours. Power deficit from the utility grid was augmented by developing a grid connected solar-hydro hybrid system.

1.5 Aim and Objectives

The aim of this research work is to develop a grid connected hybrid power system that will augment the power supply to consumers. In order to achieve this aim, the following itemized objectives are met:

1. Determination of the load profiling using Artificial Neural Networks (ANN) based on past trend of data;

2. Development of a solar-hydro hybrid system using MATLAB/Simulink Environment;
3. Integrating the developed hybrid system with the utility grid.

1.6 Methodology

The sequential steps adopted for the development of the grid connected Solar-Hydro hybrid system are:

1. Collection of three years (3) data from relevant authorities:
    i. Load Demand from Transmission Company of Nigeria (T.C.N)
    ii. River flow rate and height from Kaduna state water board
    iii. Temperature, relative humidity, rainfall, wind speed, solar radiation and sunshine hours from National Meteorological Agency (NIMET)

2. Based on the data collected in item 1 above, a load profiling was carried out to project one year load demand
    i. Development of Artificial Neural Network model based on Bayesian regularization algorithm;
    ii. Training, testing and validation of the developed model using utility data;
    iii. Forecasting the future load demand using collected data.

3. Design of solar photovoltaic module configuration;

4. Development of a hydro system using self-induction generation;

5. Development of a hybrid system (model) using items 3 and 4 above on a Simulink interface;

6. Interfacing the hybrid system with the utility via an phase lock loop;

7. Validating the developed model with other standard works.

1.7 Justification of Research

The amount of power allocated to Kaduna State has been shared to different areas of the State is less than the load demand. This in turn lead to load shading by the utility to balance the load demand with the allocated power. The load shading affects the quality, quantity and security of the system. This brought the need to develop a system capable of supplementing the allocated power to Kaduna North from the grid. Many researchers worked on developing a system to augment the deficit of power in the grid without considering the future load demand. Most of the literatures only considered limited renewable energy sources for supplementing the grid power supply, hence, the renewable energy sources available are not fully exploited. This research work addresses these problems by first forecasting the future load demand for Kaduna North and then developing a Solar-Hydro hybrid generation system to argument the deficit power obtained from the load forecast.

1.8 Dissertation Organization

In chapter one, general background and the concept of hybrid system is presented, followed by challenges facing Nigeria power system. In chapter two, a concise review of the fundamental concepts and literature review on hybrid system are presented. In chapter three, methods and materials are presented which comprise the mathematical models and Simulink models of the hybrid system. In chapter four, result was presented based on the analysis of the load profiling and solar-hydro hybrid model. Chapter five presents the conclusion, recommendation and limitations of the entire research work.

CHAPTER TWO

LITERATURE REVIEW

2.1 Introduction

This chapter reviews the fundamental concept, theoretical background relevant to the study and the review of related works.

2.1.1 Review of Fundamental Concepts

The fundamental concepts regarding the research work which includes hybrid system and forecasting are discoursed.

2.1.2 Hybrid System

A hybrid power system combines two or more methods of electricity generation, usually using renewable technologies such as solar photovoltaic, wind turbines and hydro power sources. Hybrid systems provide a high level of energy security through the mix of generation methods (Hogue *et al*, 2012). In this work, the hybrid system consists of solar photovoltaic system and hydro power system.

2.1.2.1 Solar Photovoltaic Power System Technology and Configuration

A solar cell is an electrical device that converts the energy of sun/light directly into electricity. Solar cell is the basic fundamental component of a photovoltaic system which converts the solar energy into electrical energy (Puppala and Ebraheem, 2012). Photovoltaic system configuration can be either grid connected or standalone (Ngo, 2010). In grid connected solar photovoltaic systems, the direct current (DC) output from the solar array is fed into an inverter for conversion

from direct current to alternating current (AC) before feeding into the grid. Standalone systems also use inverter for alternating current loads on the system.

2.1.2.2 Sizing of the Solar Array

Before sizing the array, the total daily energy or demand in Watt-hours (E), the average sun hour per day T_{min}, and the dc-voltage of the system (V_{DC}) must be determined. Once these factors are made available we move to the sizing process. To avoid under sizing, losses must be considered by dividing the total power demand in $Wh.day^{-1}$ by the product of efficiencies of all components in the system to get the required energy , Er (Abu-Jaseer, 2010).

$$\mathrm{Er} = \frac{\text{Daily average consumption/demand}}{\text{product of components efficiency}} = \frac{\mathrm{E}}{\eta_{\text{overall}}} \tag{2.1}$$

The peak power is the required daily energy divided by the average sun hours per day for the geographical location T_{min}:

$$\mathrm{P_p} = \frac{\text{Daily Energy requirement}}{\text{Minimum sun peak hours per day}} = \frac{\mathrm{E_r}}{\mathrm{T}_{min}} \tag{2.2}$$

The total current needed is calculated by dividing the peak power by the system DC voltage:

$$\mathrm{I_{dc}} = \frac{\text{Peak Power}}{\text{System DC voltage}} = \frac{\mathrm{P_p}}{\mathrm{V_{dc}}} \tag{2.3}$$

Modules must be connected in series and parallel according to the need, to meet the desired voltage and current in equation (2.4) and (2.5). First the number of series modules which equals the DC voltage of the system divided by the rated voltage of each module V_r:

$$\mathrm{N_s} = \frac{\text{System DC Voltage}}{\text{One module rated voltage}} = \frac{\mathrm{Vdc}}{\mathrm{V}_r} \tag{2.4}$$

Second, the number of parallel modules which equals the whole modules current divided by the rated current of one module Ir:

$$Np = \frac{\text{Whole Module current}}{\text{Rated current of one module}} = \frac{Idc}{Ir} \quad (2.5)$$

The total number of modules N_m equals the series modules multiplied by the parallel ones:

N_m=number of series modules X number of parallel module

$$N_m = N_s \times N_p \quad (2.6)$$

2.1.3 Hydroelectric Power System

Hydro systems are systems that use flowing/falling water to turn a water turbine and by that it generate electricity (Dumitru *et al*, 2009). A Hydro system typically includes a water source which is a continuous flow of water such as a creek, waterfall, small dam or spring-fed dam, with a drop in level, and that can be wholly or partially redirected through a hydro system and a turbine turned by water acting on the blades (Dumitru *et al*, 2009).

2.1.3.1 Types of Hydroelectric Power Plants and Turbines

There are three types of hydro power plants facilities: Impoundment, diversion and pumped storage (Dorin *et al*, 2012).The three classification of hydroelectric power plant based on size are large hydropower, small hydropower and micro hydropower. Hydro-turbines are classified based on the head which are reaction turbines and impulse turbines. Turbines are wheels driven by some fluid in movement that makes them rotate by action of the energy contained in them (potential or kinetic form) on slats that can have several formats (Felix and Godoy, 2006). The following are types of turbines (Felix and Godoy, 2006).

1. Pelton turbine (PT): A Pelton turbine is a turbine of free flow (action). In small hydroelectric power plants, operation of a Pelton turbine can result in reasonable economy when it operates with flows above 30 liters/sec and heads from 20m downward direction (Felix and Godoy,

2006). The necessary combination of head with design flow rate of water to obtain a requisite Pelton turbine power is shown in Figure 2.1;

2. Francis turbine (FT): The field of application of Francis turbine in small hydroelectric power plants is from 3 to 150 m of height and from 100 liters/sec of design flow of the moving water as shown in Figure 2.1 (Felix and Godoy, 2006). According to local conditions, the turbine shaft can be horizontal or vertical. The horizontal position is the most suitable, because it eases direct connection to generators (synchronous or asynchronous) (Felix and Godoy, 2006);

3. Michel–Banki (MB) turbine**:** Michel–Banki (also called radial thrust) turbines currently manufactured have a capacity of up to 800 kW (Felix and Godoy, 2006). Their flows vary from 25 to 700 liters/sec (according to the machine dimensions), with head heights in the range 1 to 200 m;

4. Kaplan (KT) or propeller hydraulic turbine: A Kaplan turbine is related to low heads or water stream, limited power, and optimum flow variations during the year and is recommended for heads from 0.8 to 5 m, approximately (Felix and Godoy, 2006);

5. Deriaz turbine (DT): When a turbine is neither radial nor axial, it is known as being of mixed flow, diagonal or semiaxial (Felix and Godoy, 2006). The thrusting water follows an approximately conic surface around the runner. A Deriaz turbine flows vary broadly from 1.5 to 250 m^3/s with head heights in the range 5 to 1000 m;

The choice of turbine type depends on the application range, primarily on height and water flow and other criteria, such as maintenance, turbine cost and sensitivity to materials in suspension (Felix and Godoy, 2006). Each turbine has its range of operation, head range and specific speed range. Figure 2.1 shows the application ranges of turbines used in hydropower plant and Table 2.1 depicts the various types of turbines with their corresponding head and speed range.

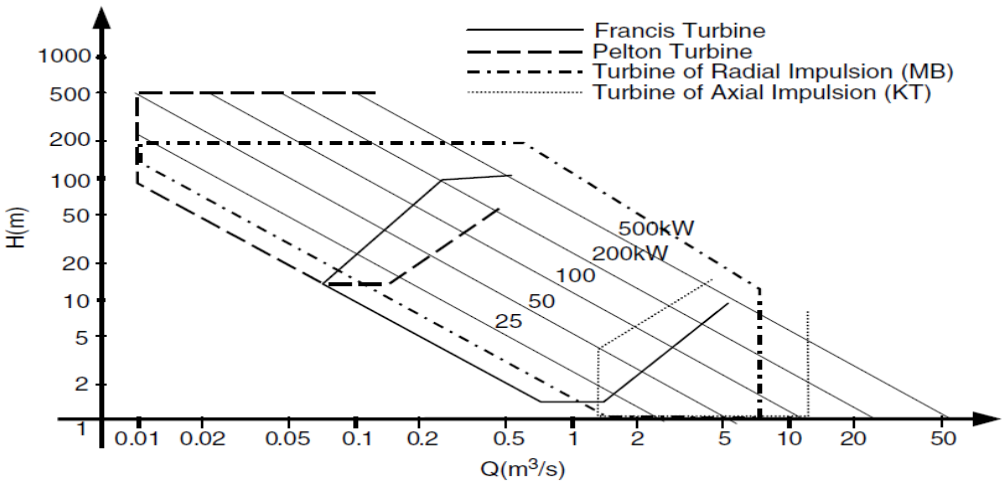

Figure 2.1: Application Ranges of Turbines (Felix and Godoy, 2006)

The various types of turbine runners, head associated with each and the speed range is shown in Table 2.1 below.

Table 2.1: Head Range and Specific Speed Ranges for Various Types of Turbine Runners (Felix and Godoy, 2006)

S/N	Turbine Runner	Head Range (m)	$n_{s\ Range}$ (rev/sec)
1	Pelton	400-2000	0-30
2	Francies	50-500	20-120
3	Mixed-Flow	20-80	120-180
4	Kaplan(vertical)	8-50	180-260
5	Buib pit or Tube (Horizontal)	0-10	260-360
6	Michel-Banki	1.50-150	30-210

2.1.3.2 Model of Hydroelectric Power System

Hydroelectric power plants harness the falling water kinetic energy to generate electricity such that turbines are used to transform falling water kinetic energy into electricity (Dorin *et al*, 2012). Water flows within a river from higher geodesic site to a lower geodesic site due to gravitation which is characterized by different particular kinetic and potential energy at both sites

(Dorin *et al*, 2012). The correct identification of the resulting energy difference of the out-flowing water can be assumed by considering a stationary and friction-free flow with incompressibility. The hydrodynamic Bernoulli pressure equation applied in such condition is given by equation (2.7) (Dorine *et al*, 2012):

$$P + \rho_w gh + \frac{1}{2}\rho_w {V^2}_w = Constant \tag{2.7}$$

Where:

P : Hydrostatic pressure;

ρ_w : Water density;

V : Velocity of the water flow;

h : Head of the turbine;

g : Acceleration due to gravity.

Equation (2.7) can be transformed so that the first term on the RHS expressed the pressure level, the second term the level of the site and the third term the water velocity level as shown in equation (2.8):

$$\frac{P}{\rho_w g} + h + \frac{1}{2}({V^2}_w/g) = Constant \tag{2.8}$$

h : The usable head of a section of the river and it is determined by considering the difference in pressure, the geometric difference in height and flow velocity of the water using equation (2.9):

$$h = \frac{P_{up} - P_{dn}}{\rho_w g} + \left(h_{up} - h_{dn}\right) + \frac{{V^2}_{w,up} - {V^2}_{w,dn}}{2g} \tag{2.9}$$

where:

P_{up} : Upstream hydrostatic pressure;

P_{dn} : Downstream hydrostatic pressure;

h_{up} : Upstream geodesic water height (head water);

h_{dn} : Downstream geodesic water height (Tail water);

$V^2{}_{w,up}$: Upstream water velocity;

$V^2{}_{w,dn}$: Downstream water velocity

The power of water supply P_w can be determined (Dorine *et al*, 2012) using equation (2.10):

$$P_w = \rho_w g q_w h_{util} \tag{2.10}$$

where:

h_{util} : Usable head of the turbine;

Considering two specific points of a river, the theoretical power Pw, th can be calculated using:

$$P_{w,th} = \rho_w g \dot{q}_w \, (h_{up} - h_{dn}) \tag{2.11}$$

For a real case scenario, in which the energy balance is considered between two specific points of a river, and also losses are incorporated, then the hydrodynamic Bernoulli equation can be written according to equation (2.12):

$$\frac{P_{up}}{\rho_w g} + h_{up} + \frac{V^2{}_{w,up}}{2g} = \frac{P_{dn}}{\rho_{w,dn} g} + h_{av} + \frac{V^2{}_{w,dn}}{2g} + \xi \frac{V^2{}_{w,dn}}{2g} = Constant \tag{2.12}$$

These energy losses are normally represented by the part of the rated power which is converted into ambient heat by friction and cannot be used technically. In the turbine, pressure energy is converted into mechanical energy and the conversion losses are described by the turbine efficiency η_t (Dorine *et al*, 2012). The usable water power that can be converted into mechanical energy at the turbine shaft is given by equation (2.13):

$$P_t = \eta_t \rho_w g \dot{q}_w h_{util} \tag{2.13}$$

where:

P_t : Turbine power

η_t : Turbine efficiency

2.1.4 Self-Excited Induction Generator (SEIG)

A 3-phase, Δ-connected induction machine has been used for converting hydro power into electrical power (Meshram *et al*, 2013). The induction machine driven by constant speed prime mover is used and operated as a Self-Excited Induction Generator (SEIG) (Meshram *et al*, 2013). The reactive power requirement of the SEIG is met by the 3-Φ excitation RLC circuit connected across the stator terminals. The elementary difficulty with the SEIG is its incapability to control the generated terminal voltage and frequency under varying load condition (Meshram *et al*, 2013). An external source of reactive current is required for terminal voltage regulation of the SEIG with varying load and to utilize the machine to its rated capacity. The utility grid is considered as a reactive current source for SEIG. The schematic diagram of hydro power plant is as shown in Figure 2.2.

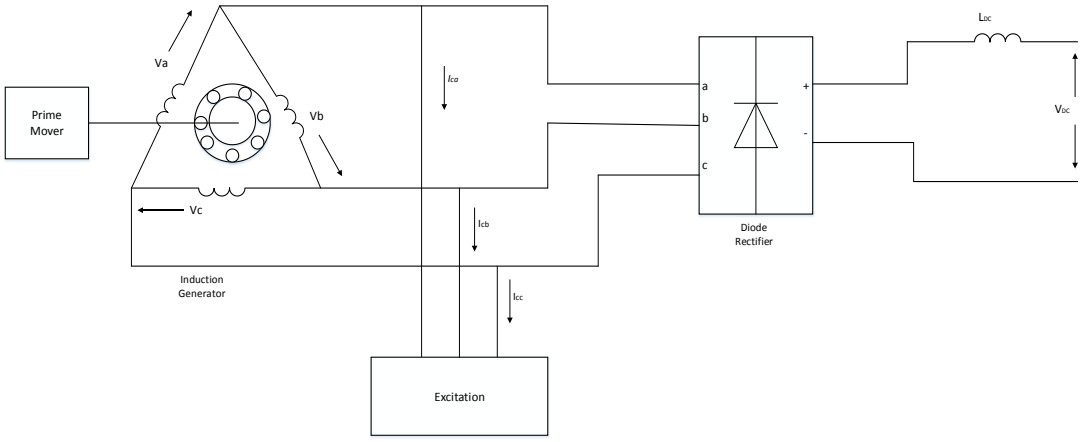

Figure 2.2: Schematic Diagram of Hydropower Plant (Meshram *et al*, 2013).

2.1.4.1 Model of Self-Excited Induction Generator (SEIG)

The dynamic model of the three phase self-excited induction generator is developed using the stationary d-q reference frame. The concerned equations are as shown in equations (2.14) to (2.22) (Meshram *et al*, 2013):

$$[v] = [R][i] + [L] * p[i] + \omega[G][i] \tag{2.14}$$

The current derivative can be expressed as:

$$p[i] = [L]^{-1}\{[v] - [R][i] - \omega[G][i]\} \tag{2.15}$$

where:

$$[v] = [v_{ds} \quad v_{qs} \quad v_{dr} v_{qr}]^T \tag{2.16}$$

$$[i] = [i_{ds} \quad i_{qs} \quad i_{dr} i_{qr}]^T \tag{2.17}$$

$$[R] = diag[R_s \quad R_s \quad R_r R_r] \tag{2.18}$$

$$L = \begin{bmatrix} L_{ls} + L_m & 0 & L_m & 0 \\ 0 & L_{ls} + L_m & 0 & 0 \\ L_m & 0 & L_{lr} + L_m & 0 \\ 0 & L_m 0 & L_{lr} + L_m & \end{bmatrix} \tag{2.19}$$

$$G = \begin{bmatrix} 0 & 0 & 0 & 0 \\ 0 & 0 & 0 & 0 \\ 0 & -L_m & 0 & -L_{lr} - L_m \\ L_m & 0 & L_{lr} + L_m & 0 \end{bmatrix} \quad (2.20)$$

The three phase stator variable is transformed into the stationary reference frame using abc to dq transformation.

$$V_{dqo} = [k][V_{abc}] \quad (2.21)$$

where:

$$k = \frac{2}{3}\begin{bmatrix} cos & cos(-\Phi) & cos(+\Phi) \\ sin & (-\Phi) & (+\Phi) \\ 1/2 & 1/2 & 1/2 \end{bmatrix} \quad (2.22)$$

2.1.5 DC-DC Boost Converter

A boost converter increases voltage level from the photovoltaic natural DC voltage to the desired DC voltage (Meshram *et al* 2013). The output voltage of the photovoltaic cell is very limited, which is very low for the application (Meshram *et al* 2013). The series and parallel combination also do not provide the required output. Hence, the boost converter is necessary to boost the low output voltage of photovoltaic array. The boost converter is as shown in Figure 2.3:

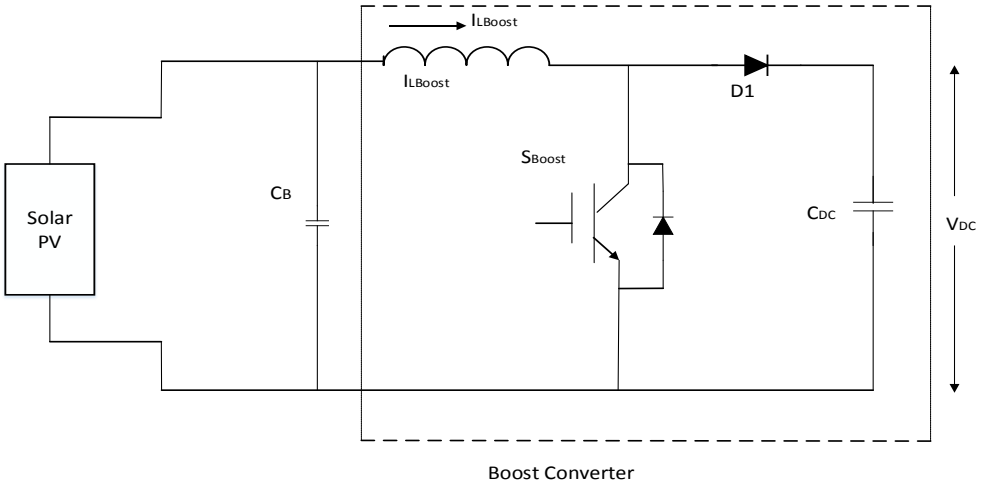

Figure 2.3:Schematic Diagram of Solar Power Plant with Boost Converter (Meshram *et al* 2013).

The DC-DC boost converter consist of switching-mode device having two semiconductor switches (a rectifier diode and a power transistor with its corresponding anti-parallel diode) and two energy storage devices (an inductor and a capacitor) for producing an output DC voltage at a level greater than its input DC voltage (Marquez *et al*, 2009). The steady state voltage and current relations of the boost converter operating in continuous conduction mode are given by (Marquez *et al*, 2009):

$$V_d = \frac{V_g}{(1-D)} \tag{2.23}$$

$$I_d = (1 - D)I_L \tag{2.24}$$

where:

I_L: Chopper input current (Inductor current)

V_d: Output voltage (DC link voltage)

V_g: Boost converter input voltage

I_d: Chopper output current

D: Duty cycle of the DC-DC converter

2.1.6 Universal Bridge Inverter

The universal bridge converter has been an important reference in the power electronics converter technology development (Teodorescu *et al*, 2011). It has a configuration consisting of force-commuted semi-conductor devices (thyristor) as shown in Figure 2.4. The universal bridge topology is very versatile, being able to be used for both DC-DC and DC-AC conversion and can also be implemented in full-bridge (FB) form with two switching legs or half bridge form with one switching leg (Teodorescu *et al*, 2011).

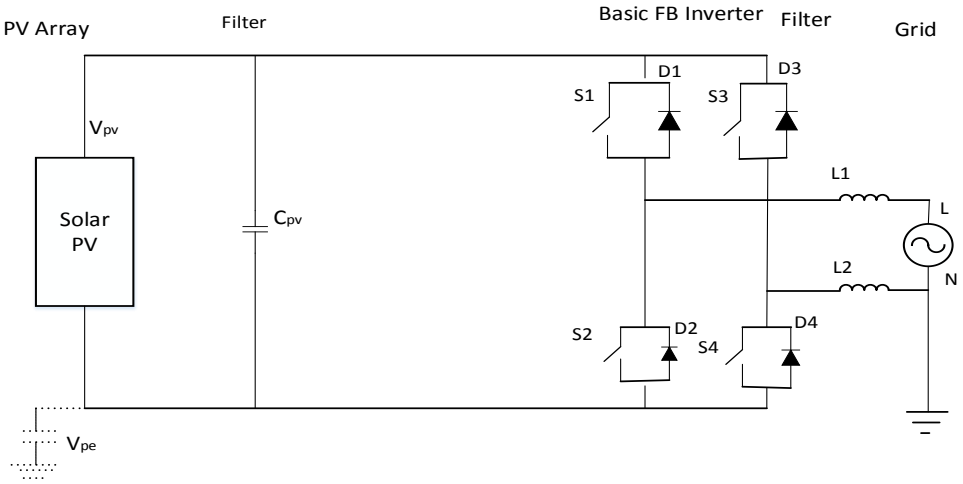

Figure 2.4: Basic Full-Bridge Inverter (Teodorescu *et al*, 2011).

2.1.7 Phase Locked Loop

The use of phase locked loop (PLL) is a major technique adopted for grid connected systems. The phase locked loop causes one signal to track another and keeps the output signal synchronized with a reference input signal in frequency and phase (Ciobotaru, 2011). In three phase grid connected system, phase locked loop is achieved after transforming Vabc to d-q and with a proper design of a loop filter. Phase locked loop is used to generate unit sine and cosine signals synchronized to system frequency from the utility voltage (Ciobotaru, 2011). Closed loop control of power converters in synchronous reference frame method needs these unit sine and cosine signals to compute feedback and modulating signals generation. The basic structure of the phase locked loop is as shown in Figure 2.5

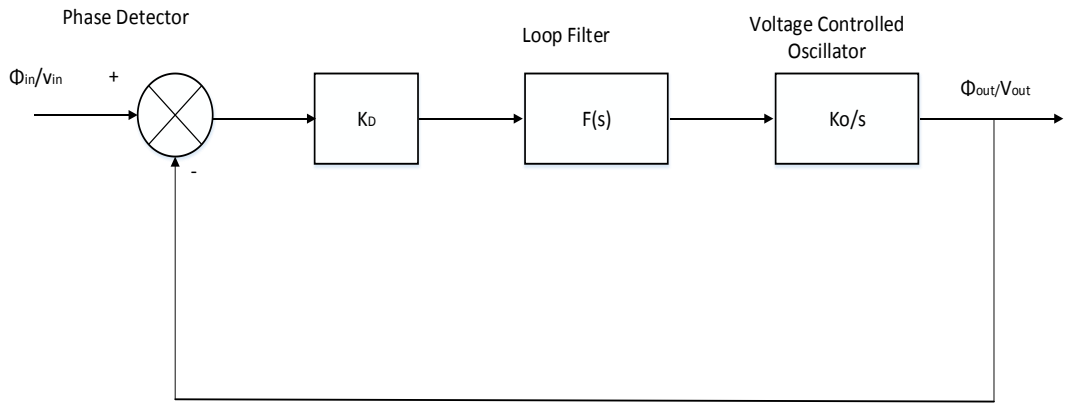

Figure 2.5: Basic Structure of Phase Locked Loop (Ciobotaru, 2011).

The phase detector generates an output signal proportional to the phase difference between the input signal Φ_{in} and the signal generated by the internal oscillator of the phase locked loop Φ_{out} producing high frequency AC component together with the DC phase-angle difference signal (Ciobotaru, 2011). The loop filter presents a low-pass filtering characteristic to attenuate the high frequency AC components from the phase detector output (consist of either first order filter or PI controller (Ciobotaru, 2011). The voltage controlled oscillator generates at its output an AC signal whose frequency is shifted with respect to a given central frequency ω as a function of input voltage provided by the loop filter (Ciobotaru, 2011).

2.1.7.1 Principle of Operation of Phase Locked Loop

Phase locked loop system is a feedback system with a regulator tracking the phase angle with input of three phases of grid voltage and output of phase angle of one of the three phases as shown in Figure 2.6 (Ogren, 2011):

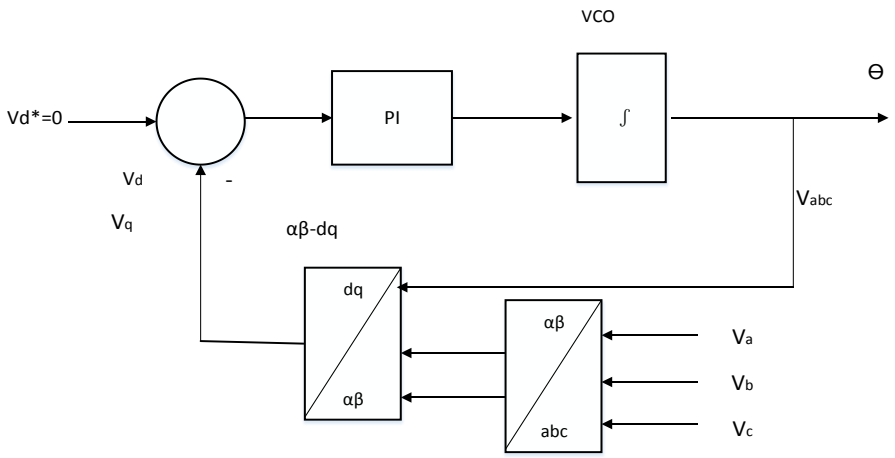

Figure 2.6: General Structure of Three Phase d-q PLL (Ogren, 2011)

Vabc is sensed from the grid and transformed into dq components using coordinate transformation abc - dq and the phase locked loop gets locked by setting Vd* to zero (Ogren, 2011). The loop filter PI is a low pass filter used to suppress high frequency component and provide DC controlled signal to the voltage controlled oscillator which acts as integrator (Ogren, 2011). The output of the PI controller is the inverter output frequency that is integrated to obtain inverter phase angle Θ. When the difference between the grid phase angle and the inverter phase angle is reduce to zero, phase locked loop becomes active which result in synchronously rotating voltages Vd = 0 and Vq gives magnitude of grid voltage (Ogren, 2011).

The transformation from three phases to two phases is necessary in order to track the phase angle. The grid voltages are given as (Ogren, 2011):

$$v_a = v_m \sin(\omega t) \tag{2.25}$$

$$v_b = v_m \sin\left(\omega t + \frac{2\pi}{3}\right) \tag{2.26}$$

$$v_c = v_m \sin\left(\omega t - \frac{2\pi}{3}\right) \tag{2.27}$$

The transformation is achieved using Park's transformation. Park's transformation is a well known three phase to two phase transformation (Dan, 2008) as shown in Figure 2.7.

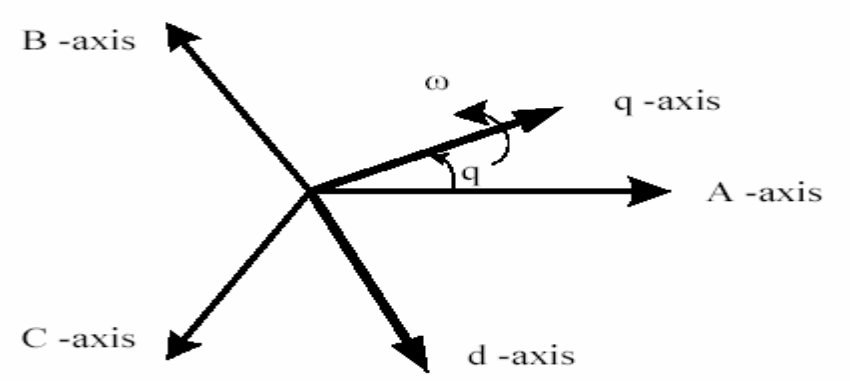

Figure 2.7: Park's Transformation

The Park's transformation equation is of the form:

$$[V_{qdo}] = T_{qdo}()[V_{abc}] \tag{2.28}$$

$$V_{qdo}() = \frac{2}{3}\begin{bmatrix} cos(\omega t) & cos\left(\omega t - \frac{2\pi}{3}\right) & cos\left(\omega t + \frac{2\pi}{3}\right) \\ \sin(\omega t) & sin\left(\omega t - \frac{2\pi}{3}\right) & sin\left(\omega t + \frac{2\pi}{3}\right) \\ \frac{1}{2} & \frac{1}{2} & \frac{1}{2} \end{bmatrix} \tag{2.29}$$

where:

ωt : Angular displacement of Park's reference frame

The three phase systems are conventionally modeled using phase notation and the transformation from equation (2.29) is presented in equations (2.30), (2.31), and (2.32):

$$v_d = \frac{2}{3}(v_a \sin(\omega t) + v_b \sin\left(\omega t - \frac{2\pi}{3}\right) + v_c \sin\left(\omega t + \frac{2\pi}{3}\right) \tag{2.30}$$

$$v_q = \frac{2}{3}\left(v_a \cos(\omega t) + v_b \cos\left(\omega t - \frac{2\pi}{3}\right) + v_c \cos\left(\omega t + \frac{2\pi}{3}\right)\right) \quad (2.31)$$

$$v_o = \frac{1}{3}(v_a + v_b + v_c) \quad (2.32)$$

where:

ω: Rotating speed

v_a,v_b and v_c: Grid phase voltages

2.1.7.2 Model of Phase Locked Loop

The phase locked loop is assumed to be locked to a reference signal (Figure 2.6) and we examine how the output varies with the loop transfer function and the input. A frequency domain approach describing transfer functions in the s-domain is used. Voltage controlled oscillator (VOC) performs the integration of the controlled voltage and provides a factor 1/s in the loop transfer function. The transfer function is obtained as (Ogren, 2011):

$$H(s) = \frac{Forward\ path\ gain}{[1+T(s)]} \quad (2.33)$$

With unity feedback:

$$H(s) = \frac{\Phi out}{\Phi in} = \frac{K_D K_o F(s)/s}{1+K_D K_0 F(s)/s} \quad (2.34)$$

The phase error given by equation (2.33):

$$_s = \Phi_{in} - \Phi_{out} = \frac{s\Phi_{in}}{s+K_D K_o F(s)} \quad (2.35)$$

For the frequency synthesis application, there is need to have ideally perfect tracking for phase and frequency steps (Ogren, 2011). Natural frequency ω_n and a damping factor ξ are defined, which are standard control terminologies for second order system. The objective is to put the denominator of the closed loop transfer function given in equation (2.33) into standard form (Ogren, 2011):

$$s^2 + 2\xi\omega_n + \omega_n^2 \tag{2.36}$$

Dividing through by ω_n^2 yields

$$\frac{s^2}{\omega_n^2} + \frac{2\xi}{\omega_n}s + 1 \tag{2.37}$$

From equation (2.33), the denominator can be written as:

$$s^2 + \omega_n s + K_v\omega_1 \tag{2.38}$$

Comparing equation (2.36) with equation (2.38), the expressions for ω_n and ξ are given by

$$\omega_n = \sqrt{K_v\omega_1} \tag{2.39}$$

$$\xi = \frac{1}{2}\sqrt{\frac{\omega_1}{K_v}} \tag{2.40}$$

This form allows the use of standard equations to describe the transient response of the system.

The configuration of the PLL is as shown in Figure 2.8.

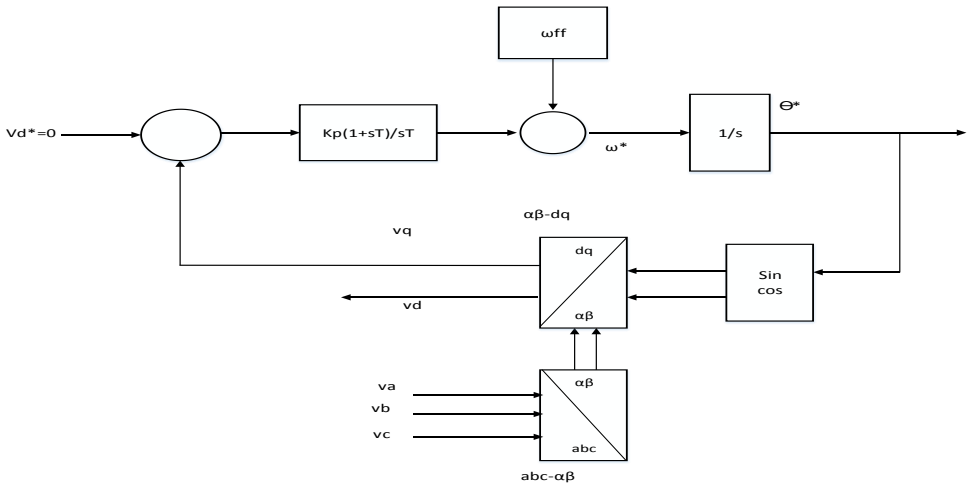

Figure 2.8: Phase Locked Loop Block Diagram (Aleksandr, 2009)

The phase voltages V_a, V_b and V_c of the grid are transformed to V_d and V_q using αβ and dq transformation. If the frequency command ω* is identical to the utility frequency, the voltages V_d and V_q appears as DC values depending on the angle Θ^* (Aleksandr, 2009). To achieve a better performance and small steady state errors in magnitude and phase, the dq frame based control are adopted (Aleksandr, 2009). A feed-forward reference ($\omega_{ff} = 2\pi f$) was also included to improve the initial dynamic performance, while f_g is the grid nominal frequency (Aleksandr, 2009).

2.1.7.3 Stationary Reference Frame

To track the phase angle, the three phase voltage signals V_a, V_b and V_c are transformed from three phases to a stationary system of two phases V_α and V_β (Rolim, 2006). The grid voltages are given as (Rolim, 2006):

$$V_a = V_m sin() \tag{2.41}$$

$$V_b = V_m sin(-\frac{2\pi}{3}) \tag{2.42}$$

$$V_c = V_m sin(+ \frac{2\pi}{3}) \quad (2.43)$$

Where Ɵis the phase angle 2πft.

The transformation is achieved using Clark's transformation. The stationary two phase variables of Clark's transformation matrix are denoted by α and $\beta, \alpha - axis$ and $\beta - axis$ are orthogonal as shown in Figure 2.9

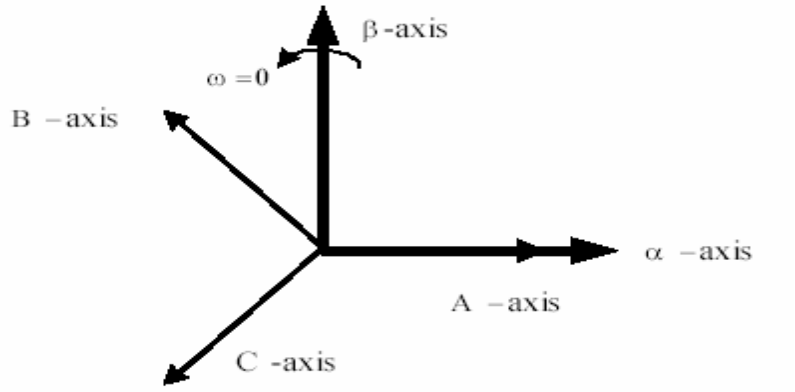

Figure 2.9: Clark's transformation

From Figure 2.9, V_α and V_β are found to be:

$$V_\alpha = V_a \quad (2.44)$$

$$V_\beta = \frac{2V_b + V_a}{\sqrt{3}} \quad (2.45)$$

In order for the transformation to be invertible, a third variable known as the zero-sequence component is added. The resulting transformation is given by equation (2.46):

$$[V_{\alpha\beta o}] = T_{\alpha\beta o}[V_{abc}] \quad (2.46)$$

The transformation matrix T is given by equation (2.47)

$$T_{\alpha\beta o} = \frac{2}{3}\begin{bmatrix} 1 & -\frac{1}{2} & -\frac{1}{2} \\ \alpha & \frac{\sqrt{3}}{2} & \frac{\sqrt{3}}{2} \\ \frac{1}{2} & \frac{1}{2} & \frac{1}{2} \end{bmatrix} \quad (2.47)$$

Similarly, the αβ-transformation matrix which gives transformation without the zero-sequence component is given by equation (2.48)

$$T_{\alpha\beta} = \frac{2}{3}\begin{bmatrix} 1 & -\frac{1}{2} & \frac{1}{2} \\ 0 & -\frac{\sqrt{3}}{2} & \frac{\sqrt{3}}{2} \end{bmatrix} \quad (2.48)$$

Carrying out the matrix multiplication $\mathrm{V}_{\alpha\beta} = T_{\alpha\beta}\mathrm{V}_{\mathrm{abc}}$ yields

$$\begin{bmatrix} V_\alpha \\ V_\beta \end{bmatrix} = \begin{bmatrix} V_m & \sin() \\ V_m & \cos() \end{bmatrix} \quad (2.49)$$

V_α and V_β are two signals carrying information about the phase angle of one of the phases, Va. The transfer function of Phase Locked Loop in Figure 2.8 is a lag and an integral element (Kaura and Blasko, 1997)

$$G_p = \left(\frac{1}{1+STs}\right)\left(\frac{1}{s}\right) \quad (2.50)$$

where:

G_p : Transfer function of the entire system

$\left(\frac{1}{1+STs}\right)$: Lag of the system

Ts: Sampling period

$\left(\frac{1}{s}\right)$: Integral element which depicts the voltage controlled oscillator.

The open and closed loop transfer functions for the system are given by equation (2.51) and (2.52) respectively (Kaura, 1997)

$$G_{ol} = \left(kp\frac{1+S\tau}{S\tau}\right)\left(\frac{1}{1+STs}\right)\left(\frac{V_m}{s}\right) \tag{2.51}$$

$$G_{cl} = \frac{G_{ol}}{1+G_{ol}} = \frac{\left(kp\frac{1+S\tau}{S\tau}\right)\left(\frac{1}{1+STs}\right)\left(\frac{V_m}{s}\right)}{1+\left(kp\frac{1+S\tau}{S\tau}\right)\left(\frac{1}{1+STs}\right)\left(\frac{V_m}{s}\right)} \tag{2.52}$$

where:

G_{ol} : Open loop transfer function

G_{cl}: Closed loop transfer function

V_m: Amplitude voltage level

V_m: Regulator gain

For the system to be able to handle discrete signal since the grid voltage signal are sampled, the system will therefore work in frequency domain with integrating elements of the plants corresponding to equation (2.53) (Kaura, 1997):

$$G(s) = \frac{F(s)}{E(s)} = \frac{1}{s} \tag{2.53}$$

Taking the derivative of equation (2.53) we obtain:

$$\frac{df}{dt} = e(t) \tag{2.54}$$

Solving equation (2.54) numerically,

$$f(t) = f(t) + \int_{to}^{t} e(t)\, dt \tag{2.55}$$

If the solution is represented in discrete points t=kTs for k = 0, 1, 2, 3…, then equation (2.55) becomes:

$$f(kT_s + T_s) = f(kT_s) + \int_{KT_s}^{KT_s+T_s} e(t)\, dt \tag{2.56}$$

Integrating equation (2.56) using Euler forward, we obtain equation (2.57). Euler forward was used because of its simplicity in implementation on second order systems in a discrete form

$$f(kT_s + T_s) = f(kT_s) + T_s e(kT_s) \tag{2.57}$$

Taking the Z-transform of equation (2.57)

$$zF(z) - F(z) = T_s E(z) \tag{2.58}$$

$$G_{int} \frac{F(z)}{E(z)} = \frac{Ts}{z-1} \tag{2.59}$$

$$S = \frac{z-1}{Ts} \tag{2.60}$$

Using equation (2.60) the PI- regulator in Z-domain is expressed as:

$$G_{pi} = kp \frac{1+S\tau}{S\tau} = Kp \frac{z-1\frac{Ts}{\tau}}{z-1} \tag{2.61}$$

To design the PI regulator gains (k_p and τ), symmetrical optimum method was used because it allows easy tuning of the PI regulator gains (Kaura and Blasko, 1997). The idea is to optimize the phase margin to have its maximum at a given cross over frequency ωd. The phase margin describes the number of degrees the frequency response may be phase shifted without losing

stability and this corresponds to the distance from the point -1 in the plot of frequency response locus shown in Figure 2.10 (Kaura and Blasko, 1997). The amplitude and phase plot should also be symmetry around ωd as shown in Figure 2.11 (Kaura and Blasko, 1997).

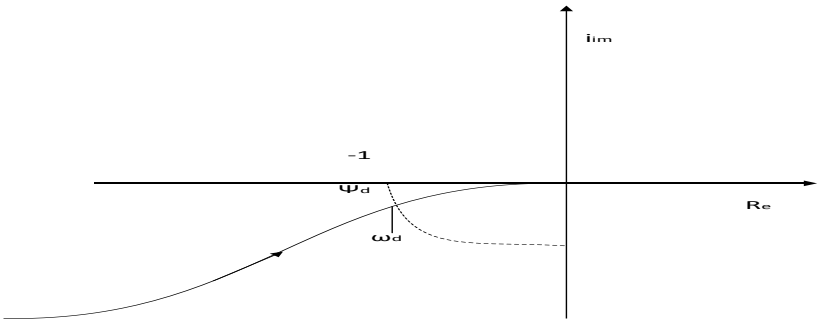

Figure 2.10: Frequency Response with Phase Margin (Kaura and Blasko, 1997)

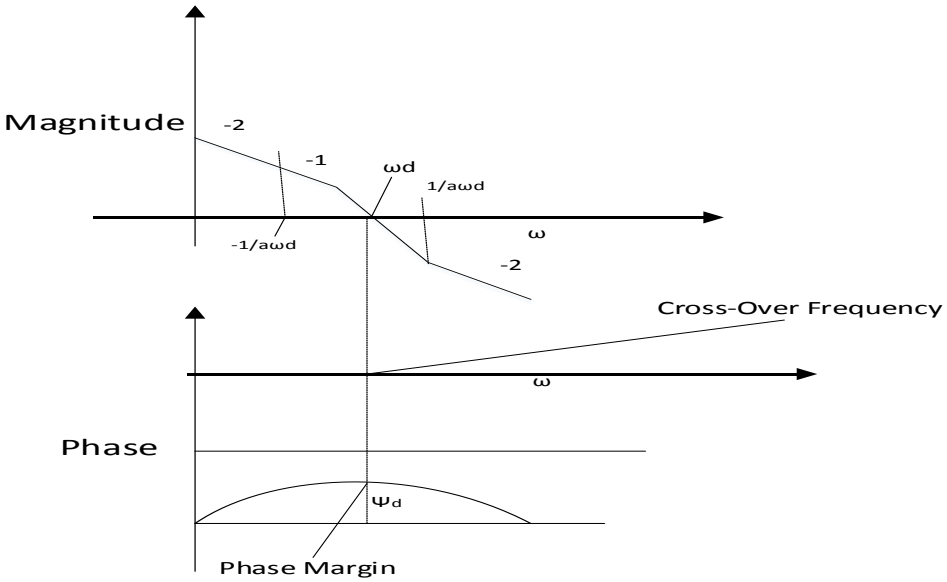

Figure 2.11: Bode Plot with Symmetry Shape at Crossover Frequency Ψ_d (Kaura and Blasko, 1997)

From the Figure 2.10, a transfer function is written as:

$$F = \frac{\omega_o^2(Ks+\omega_o)}{s^2(s+k\omega_o)} \tag{2.62}$$

where:

K: A constant that will have symmetry around ω = ωd

Rewriting the transfer function for the phase locked loop in equation (2.51) yields (Levine and William, 1999):

$$G_{ol} = \left(kp\,\frac{1+S\tau}{S\tau}\right)\left(\frac{1}{1+STs}\right)\left(\frac{V_m}{s}\right) = \frac{KV_m(s+\frac{1}{\tau})}{s^2(s+\frac{1}{T_s})} = \frac{KV_m}{aT_s}\,\frac{(as+\frac{a}{\tau})}{s^2(s+\frac{1}{T_s})} \tag{2.63}$$

Comparing equation (2.62) and (2.63), gives the following (Levine and William, 1999):

$$\begin{cases} \frac{1}{T_s} = a\omega_c \\ \frac{a}{\tau} = \omega_c \\ \frac{KV_m}{T_s} = \omega_c \end{cases} \tag{2.64}$$

where:

a: Normalization factor

ω_c: cross over frequency.

Equation (2.64) can also be written as:

$$\begin{cases} \omega_c = \frac{1}{aT_s} \\ \tau = a^2T_s \\ K_p = \frac{1}{aV_mT_s} \end{cases} \tag{2.65}$$

2.1.8 Forecasting

Forecasting is the process of making statements about events whose actual outcome have not yet been observed and therefore serves as basis of decision making (Isaac *et al,* 2014). Load forecasting is the projection of future electrical load that will be required by a certain geographical area with the use of previous electrical load usage in the said geographical area (Isaac *et al,* 2014).The main categories of load forecasting models are classical approach and artificial neural networks (Aslan *et al,* 2011). In this work, artificial neural networks approach was used. A comparative analysis for different learning algorithms was done and presented in Table 2.2 to obtain the best learning algorithm for this work.

Table 2.2: Comparative Analysis of the Different Learning Algorithms (Graupe, 1997)

S/N	TRAINING ALGORITHM	TRAINING ALGORITHM CHARACTERISTIC FEATURES AND CONVERGENCE SPEED
1	Batch gradient decent (traingd)	Slow convergence Network may get stock in a shallow local minimum Learning improvement/rate is constant
2	Batch gradient decent with momentum (traingdm)	Faster than traingd Momentum coefficient (mc) is added to (traingd) Leaning rate is also held constant For Mc=0, change is based on gradient For Mc=1, weight change is equal to last weight
3	Variable learning rate (traingdx)	Learning rate (lr) changes during training process Slope determine magnitude and direction of weight update
4	Resilient Backpropagation (trainrp)	Learning rate changes during training Magnitude of derivative have no effect on the weight update Sign of derivative shows the direction of weight update Delt-inc and delt-dec are use as size of weight change Adjustment of weight are in direction of negative gradient Perform well in pattern recognition problems
5	Conjugate gradient algorithms	Search is performed along conjugate directions Adjustment of weight depends on outcome of search direction Weight update/step size is adjusted at each iteration
6	Quasi-Newton algorithm/secant	Faster than conjugate algorithm in optimization and convergence Computation of Hessian matrix (second derivative) in Neutons method Update an approximate Hessian matrix at each iteration of the algorithm in Quasi-Newton
7	Levenberge-Marquardt (trainlm)	Second order training speed Approximate Hessian Matrix computation Requires storage of matrix that are quite large for certain problems. Perform well in function approximation problems
8	Bayesian regularization (trainbr)	Updates of weight and bias values according to Levenberg-Marquardt optimization Minimizes a combination of squared errors and weights Determines the correct combination of square errors and weight so as to produce a network that generalizes well Improves generalization High convergence speed

The model adopted the use of Bayesian regularization training algorithm for the forecasting purpose due to its simplicity, high speed of convergence, low memory usage, improve generalization and efficiency in handling both linear and non-linear data.

2.1.8.1 Bayesian Regularization Training Algorithm

Bayesian method is an optimal method for learning neural network which can automatically obtain the regularization parameters (Wang and Song, 2014). Regularization as a means of improving network generalization is used within the Levenberge Marquardt (LM) algorithm. It involves modification in the performance function (Tiwari *et al*, 2013). The performance function for this algorithm is the sum of square errors (SSE) and it is modified to include a term that consist of the sum of squares of the network weights and biases (Tiwari *et al*, 2013). Bayesian method integrates the merits of high convergence speed and prior information of Bayesian statistics (Wang and Song 2014). The network performance function / training objective function of Bayesian regularization is given by (Tiwari *et al*, 2013):

$$F = \beta SSE + SSW \tag{2.66}$$

where:

SSE and SSW are given by:

$$SSE = \sum_{q=1}^{n} e_q^2(x) \tag{2.67}$$

$$SSW = \sum_{j=1}^{n} W_j^2 \tag{2.68}$$

where:

F: Performance index;

n: Total number of weights and biases;

W: Weight

e: Error

SSE: Sum of squared network errors;

SSW: Sum of squared network weights;

and β: Regularization parameters.

The performance index F forces the weights and biases to be small, which produces a smoother network response and avoids overfitting. The main purpose of Bayesian statistic is to find the right values of α and β to implement regularization which are determined using Bayesian regularization in an automate manner (Tiwari *et al*, 2013).

2.2 Review of Similar Works

Some available similar works previously done in hybrid generation systems ware reviewed below:

Debosmita *et al.* (2005) presented a design of a grid connected hybrid system for distributed energy production. A converter was used for maximum power point tracking to maximize the power extracted from the hybrid system. However, its drawback is that one of the primary power sources is fuel cell unit which requires constant supply of hydrogen for its operation and the effect of loss of power from grid is not taken into consideration.

Dimitris *et al.* (2007) researched on standalone power system that was used for stationary applications. The work integrated photovoltaic array and wind generators for energy production from renewable energy sources. A polymer electrolyte membrane electrolyser, a polymer electrolyte membrane fuel cell, a hydrogen storage unit, a lead-acid accumulator and the power conditioning equipment were used. This work was simulated and results were obtained for only a period of two-months but this time was too short to make a precise judgment about the system. Also the work did not plan for increased load demand in future since the system is a standalone system.

Jimoh *et al.* (2007) worked on off grid connected hybrid system. It looked at the possibility of using deep cycle batteries as electrical storage means. The drawbacks of this research are that the analysis is made in off-grid (Standalone system) since greater percentages of people in the area are already connected to the grid. Lastly no plan was made to take care of additional load demand which is expected to increase as the population of the site increased.

Fei *et al.* (2010) presented their work which was based on modeling and simulation of grid connected hybrid distributed generation system. The work presented a model of a grid connected

photovoltaic/battery generation system in which all the models were simulated. However, the modeling uses only one renewable energy sources that is photovoltaic array which is intermittent and solely depends on weather condition and no plan was made to take care of future load demand in the area. The effect of loss of power from grid is not taken into consideration.

Abacha *et al.* (2011) also conducted a research on hybrid system that will supply power to remote users. In their work, the main power which comes from the hybrid system comes from the photovoltaic panels while fuel cell electrolyser and batteries are used as back up units. In this research, optimization of the system is done by hybrid optimization model for electric renewable (HOMER) software alone. Its drawback is the use of solar alone which cannot generate power during the night was used and future load demand of the remote users is not taking into consideration.

Deepak *et al.* (2011) conducted a research on Hybrid power system using hybrid optimization model for electric renewable sources. The paper focused on a hybrid power generation system suitable for remote area (Sundargarh district of Orissa State, India). The homer software is used to study and design the proposed hybrid alternative energy power system model. Sensitivity analysis was also carried out. The storage means used are battery bank. Other optimization technique need to have been incorporated so as to obtain an optimal operation of the system and future load demand was not taking into consideration.

Arun and Dilip (2012) researched on hybrid integrated renewable energy system for an isolated community. A MATLAB based computer program was developed to determine the cost effective energy source to supply the required load at any given time of the day for the community. This

system employed the use of a storage means. The researcher did not consider the possibility of population growth in that isolated community and planned for it.

Dorin *et al.* (2012) presented an isolated hybrid renewable energy system in which the components of the hybrid power system and the entire power system where modeled. They modeled each component and the entire system in an isolated mode. However, the main drawback of this system is that it only operates as a standalone system hence as the population of the area increases the system cannot cater for the deficit in load demand.

Halimeh *et al.* (2012) worked on a comparative studies on two configurations of Solar-Hydrogen hybrid energy system for standalone system using Fuzzy based particle swarm optimization algorithm. This configuration included Photovoltaic panels, fuel cell, electrolyser, hydrogen tank and batteries for storage energy. This research did not take into account, incorporating other renewable energy sources since solar radiation is unavailable in the night.

Research done by **Otun *et al.* (2012**) found that the Kangimi reservoir which lies within the sub basin of Kaduna river system can potentially generate up to 1.109MW if the turbine is placed at a height of 612m above sea level. The work only harnesses the hydropower potential of Kangimi located at the tributary of river Kaduna and fails to analyse the hydro potential of the river Kaduna itself. Also the detail of how this amount of power was generated is not evident in their work.

Hassan *et al.* (2013) presented modeling of renewable energy system using hybrid optimization model for electric renewable. It adopted the use of combined hybrid system with hydrogen electrolyser as storage means but did not consider future load demand due to growth in population and the demand for electric energy in the area.

Most of the literatures reviewed only consider limited renewable energy sources. These renewable energy sources are not fully exploited. Future load demand at the case study areas where not taken into consideration in most literatures. The main focus of this research work is to develop a grid connected hybrid system which will incorporate the stochastic nature of load growth. The system will be capable of augmenting the present shortage of power and future load demand of the proposed site.

Other available works done that are related to forecasting are reviewed below:

Mehmet and Ummuhan (2009) presented a research on next day load forecasting using artificial neural network models with auto regression and weighted frequency blocks. Two different hybrid approaches were presented. Steepest decent training algorithm was utilized to train the network. This algorithm is slow compared to other training algorithm. Steepest decent algorithm makes the network slower in convergence because sigmoid functions slope decreases as the input parameters increase so the magnitude of the slope will be very small causing small change in weight update and consequently slow convergence of the network. Weather factors are not considered such as sunshine hours, temperature, relative humidity, wind speed, rain fall and solar radiation.

Jianjun *et al.* (2010) presented a paper on medium and long term load forecasting based on dynamic architecture for artificial neural networks. A novel dynamic architecture for artificial neural network (DAN2) method was used in the load forecasting and the structure of dynamic architecture for artificial neural network was automatically formed by training and was employed to forecast. The network contains an input layer, several hidden layers and output layer. Its major drawback is that it is complex. Even though the network structure of dynamic architecture for

artificial neural network is a feed forward such that neurons in one layer are connected to the neurons of the next layer, computation of the error signal is very difficult because of the complexity of the network and that lowers the speed of convergence of the network. Also factors associated with load demand were not taken into consideration such as wind speed, sunshine hours, temperature, relative humidity, rain fall and solar radiation.

Aslan *et al.* (2011) presented a research on long term electrical peak load forecasting of Kutahya using neural networks. The long term peak load forecasting was performed with the least square regression based method and artificial neural networks. In this work, a three layer artificial neural network model feed forward-back propagation algorithm using Levenberg-Marquardt (LM) algorithm was used. The major limitation of this algorithm is the fact that Levenberg-Marquardt was designed for least square problems that are approximately linear and hence does not perform well in pattern recognition problems. Another drawback is that as the number of parameters of the network increases, the computational requirement in Levenberg-Marquardt algorithm increases geometrically which make the storage requirement of Levenberg-Marquardt larger than other algorithms.

Bassaran *et al*. 2011presented a work on forecasting of electric energy demand using novel mathematical models and neural networks. Three artificial neural networks structures were developed and tested for achieving small forecasting errors. All the networks use Levenberg-Marquardt as learning algorithm. The result obtained from the neural network provides specified models that are better fine-tuned for the available data and have best forecasted result. The drawback of this three artificial neural networks lies on the selection of Levenberg-Marquardt as learning algorithm because speed of convergence and accurate prediction in Levenberg-Marquardt algorithm decreases as the number of network parameters (weights and biases)

increases. The storage requirements of Levenberg-Marquardt are large, but by adjusting the mem_reduc parameter, the storage requirements can be reduced although at a cost of increased execution time.

Hussein and Kamel (2011) worked on Shannon entropy and mean square errors for speeding the convergence of Multilayer Neural Networks (comparative approach). The mean square error (MSE) minimization principle of multilayer back propagation (BP) was substituted by the minimization of Shannon entropy (SE) of the difference between the multilayer perceptron output and the desired target. The two cost functions are studied, analyzed and tested with two different activation functions which are the Cauchy and the hyperbolic tangent activation function. The drawback of each is that the convergence is relatively slow in Shannon entropy approach. Many environmental factors that have effect on the model were not considered such as temperature, relative humidity, rain fall, solar radiation and sun shine hours.

Samsher and Unde (2012) worked on load forecasting using artificial neural networks technique based on multilayer perceptron. The training algorithm used in the work was conjugate gradient algorithm. The drawback of this work lies on the type of training algorithm selected. For a gradient decent algorithm, a line search is required at the end of each iteration. The line search is computationally expensive and time consuming since it requires the network response to all training inputs be computed several times for each search. The forecasting did not consider factors that affect load demand in an area such as temperature and rainfall.

Naveen (2013) presented a paper on electrical load prediction using artificial neural network for the purpose of predicting the future load. The prediction model is trained by historical data from electrical utility. A three layer feed forward neural network, trained by using back propagation

method based on Levenberg-Marquardt algorithm. The set back of this algorithm is that it is complex and expensive to compute approximate Hessian matrix. By using this algorithm, when the error on the training set is driven to a very small value, and a new data is presented to the network, the error becomes large. This shows that the network has memorized the training examples but has not learned to generalize to the new situation. This signifies that the network has overfit.

Saeed and Ossama (2013) presented on forecasting electrical load using artificial neural network combined with multiple regression method to predict electrical load for a specific day, week and month. The technique was compared with extrapolation of trend curves as a traditional method (linear regression models). The training algorithm used was based on Broyden, Flecher, Goldfarb and Shanno (BFGS). This training algorithm is among the faster training algorithm and faster than both steepest decent and conjugate gradient algorithm. Its major limitation is that the training algorithm is very complex and expensive to compute approximate Hessian matrix for the feed forward networks and the algorithm also requires large storage. Another drawback of this training algorithm is that during network training, the network tends to overfit. Effects of environmental factors were not considered such as temperature and solar radiation.

A lot of work has been done in the area of forecasting load demand both in classical approaches and artificial neural networks. Most of the classical approaches suffer from slow convergence speed. Research in load forecasting using artificial neural networks has achieved a milestone by using a feed-forward back propagation networks using different training algorithms. But the training algorithms used in most work converge slowly such as batch gradient decent, batch gradient decent with momentum and variable learning rate algorithms while other faster training algorithms suffer from complexity, high memory requirement and overfitting such as quasi-

newton and levenberg-marquardt algorithms. In this work, forecast was achieved using Bayesian regularization which has high convergence speed and improved generalization.

CHAPTER THREE

MATERIALS AND METHODS

3.1 Introduction

This chapter discusses the methodology adopted and the sequential steps of the developed approach accompanied with the Simulink implementation of the developed model.

3.2 Load Profiling

The load forecasting was done using artificial neural network based on Bayesian regularization algorithm to determine the load demand trend, so as to project the next year load demand. Matlab code was developed as shown in Appendix A for the purpose of the forecasting. The model considered load demand and environmental conditions as contained in Figure 3.1.

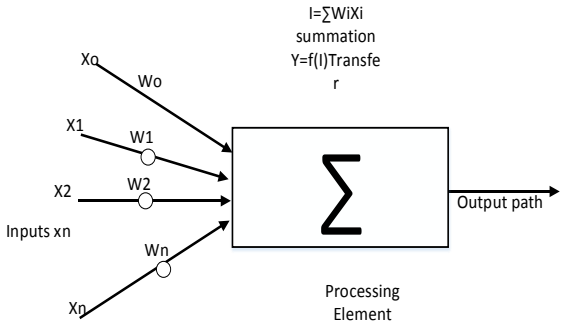

Figure: 3.1 Model Architecture of the Neural Network

The model comprises of the weight vector, the bias, input weights, input bias and the output. The model of Figure 3.1 is described by equation (3.1):

$$F(X) = \sum_1^n XW + XoWo \tag{3.1}$$

Where:

Xo: Bias;

Wo: Weight of the bias;

X_1 to X_n: Input parameters;

W_1 to W_n: Weights of the input parameters;

$F(X)$: Output.

The environmental factors considered are temperature, relative humidity, rainfall, solar radiation and sunshine hours and equation (3.1) becomes equation (3.2)

$$F(X) = PW_1 + TW_2 + HW_3 + RW_4 + WW_5 + SW_6 + SSW_7 + X_O W_O \quad (3.2)$$

Where:

P: Load demand and W_1 is the weight assigned to the load demand;

T: Temperature and W_2 is the weight assigned to temperature;

H: Relative humidity and W_3 is the weight assigned to humidity;

R: Rainfall and W_4 is the weight assigned to rainfall;

W: Wind speed and W_5 is the weight assigned to wind speed;

S: Solar radiation and W_6 is the weight assigned to solar radiation;

SS: Sunshine hours and W_7 is the weight assigned to sunshine hours.

The model adopted was based on Bayesian regularization algorithm for the forecasting purpose due to its simplicity, high speed of convergence, low memory usage; improve generalization and efficiency in handling both linear and non-linear data. The detail of how the model was developed is depicted in the flowchart of Figure 3.2 and its Matlab code is contained in Appendix A.

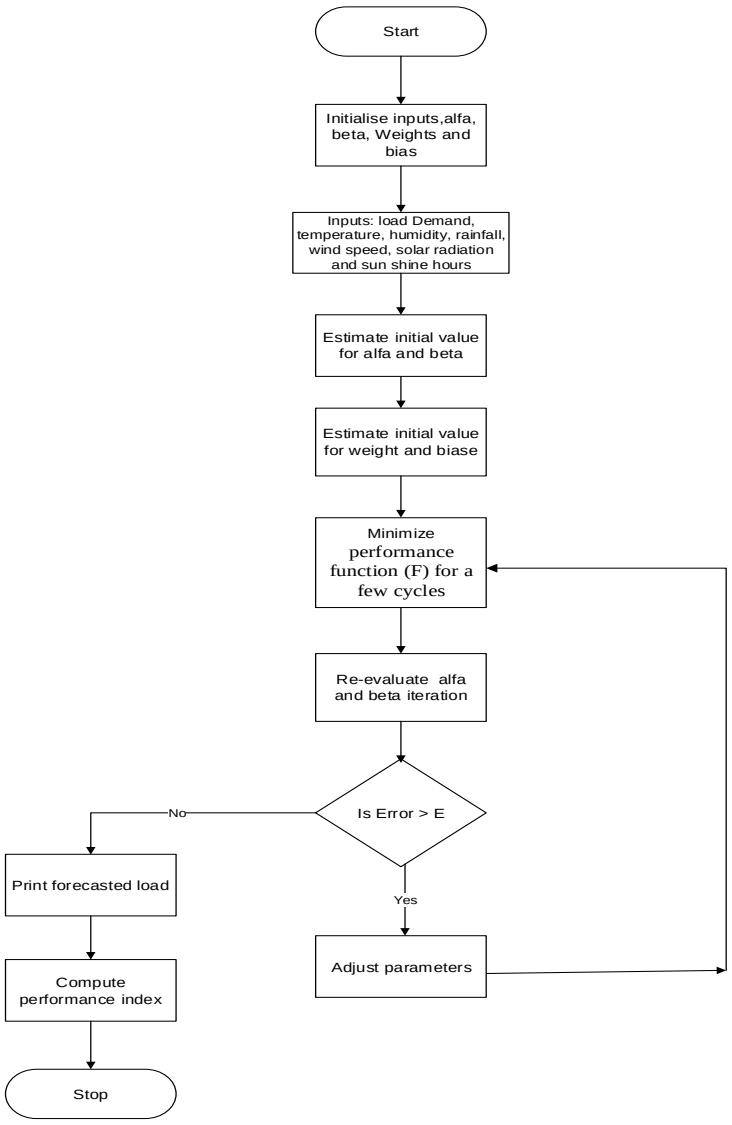

Figure 3.2: Flowchart of the Developed Artificial Neural Network Model

Where E is the minimal error which minimized the performance index (F(x))

3.3 Developed Hybrid Model

The developed model comprises a solar photovoltaic system and hydropower system. The output voltage of the photovoltaic system was first boosted using a DC-DC boost power converter. The Hydropower system AC voltage was converted to DC voltage using universal AC-DC converter

before connected to the photovoltaic system. The hybrid system was interfaced to the grid via a DC-AC inverter, step-up transformer and phase locked loop system as highlighted in Figure 3.3.

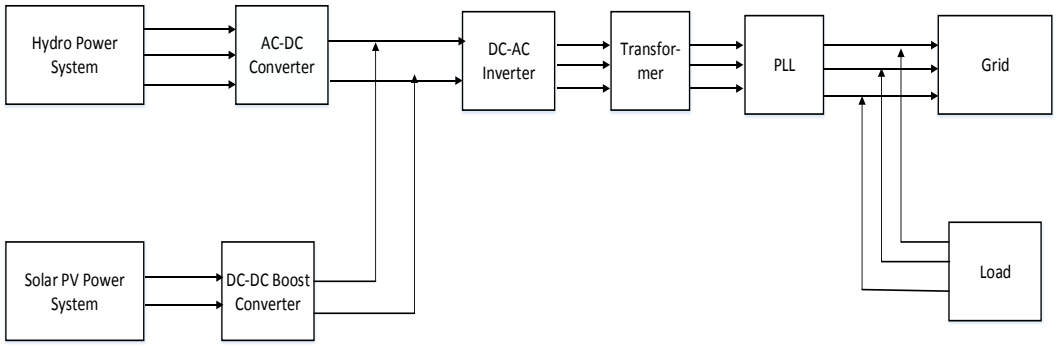

Figure 3.3 Hybrid System Configuration

The two ways to integrate hybrid system into the grid are AC link and DC link. In this work, simulation modeling of the grid connected hybrid system was done using DC linked bus bar. Figure 3.3 shows the schematic diagram of the grid connected DC linked solar-hydro hybrid system. The power from the grid system acts as a dominant system and the hybrid system acts as supplementary system to compensate grid deficit power.

3.4 Solar Photovoltaic System Model

Solar photovoltaic system utilizes Solarex MSX64 photovoltaic cell to generate electricity due to its portability, availability and low cost. Solarex MSX64 is a solar photovoltaic cell that produces output power of 80W per photovoltaic cell. It has the following electrical characteristics as shown in Table 3.1.

Maximum Power (Pm)	**84 W**
Voltage @ P_{max} (V_m)	17.5 V
Current at @ P_{max} (I_m)	4.66A

Table 3.1: Electrical Characteristics of MSX 64 Photovoltaic Module (Dorine *et al*, 2009).

Guaranteed Minimum P_m	80W
Short Circuit current (I_{sc})	4.21a
Open Circuit voltage (V_{oc})	21.3A
Temperature co-eff of V_{oc}	-(80±10) mV/ C
Temperature co-eff of Isc	(0.065±0.15) %/^{o}C

A monthly average solar radiation of Kaduna north of 653.45W/m^2 (NIMET) was used as the solar irradiance for the developed photovoltaic model.

3.4.1 Sizing the Photovoltaic Array

The sizing of the photovoltaic array was done based on the following design parameters:

Power required from the solar system = Peak power =330kW

System DC Voltage = 1400V

1400V DC was selected because it is the input voltage required by the boost converter.

System current was obtained using:

$$I_{dc} = \frac{Peak\ Power}{System\ DC\ Voltage} \tag{3.3}$$

$$I_{dc} = \frac{330000}{1400} = 235.7143A$$

The number of modules in series is given by:

$$N_s = \frac{System\ DC\ Voltage}{One\ module\ rated\ voltage} \tag{3.4}$$

$$N_s = \frac{1400}{17.5} = 80$$

Similarly the number of modules in parallel is

$$N_p = \frac{Module\ Current}{Rated\ Current\ of\ One\ Module} \tag{3.5}$$

$$N_p = \frac{235.7143}{4.66} = 50$$

Therefore, No. of modules is equal to

$$No.of\ modules = N_s * N_p \tag{3.6}$$

$$No.of\ modules = 80 * 50 = 4000modules$$

3.4.1.1 Model of Photovoltaic Array

The mathematical relationship for the current in the single-diode equivalent circuit is described using equation (3.7) (Chen *et al*, 2013):

$$I_{pv} = I_{sc}\left\{1 - C_1\left[exp\left(\frac{V_{mp}}{C_2 V_{oc}}\right) - 1\right]\right\} \tag{3.7}$$

Where C1 is given by:

$$C_1 = \left(1 - \frac{I_{mp}}{I_{sc}}\right) exp\left[\frac{-V_{mp}}{C_2 V_{oc}}\right] \tag{3.8}$$

And C2 is given by:

$$C_2 = \frac{\frac{V_{mp}}{V_{oc}} - 1}{In\left(1 - \frac{I_{mp}}{I_{sc}}\right)} \tag{3.9}$$

Where:

I_{pv}: Solar photovoltaic cell current

I_{sc}: Short circuit current

V_{pv}: Solar photovoltaic cell voltage

V_{oc}: Open circuit voltage

Figure 3.4 shows the standard model for a photovoltaic array.

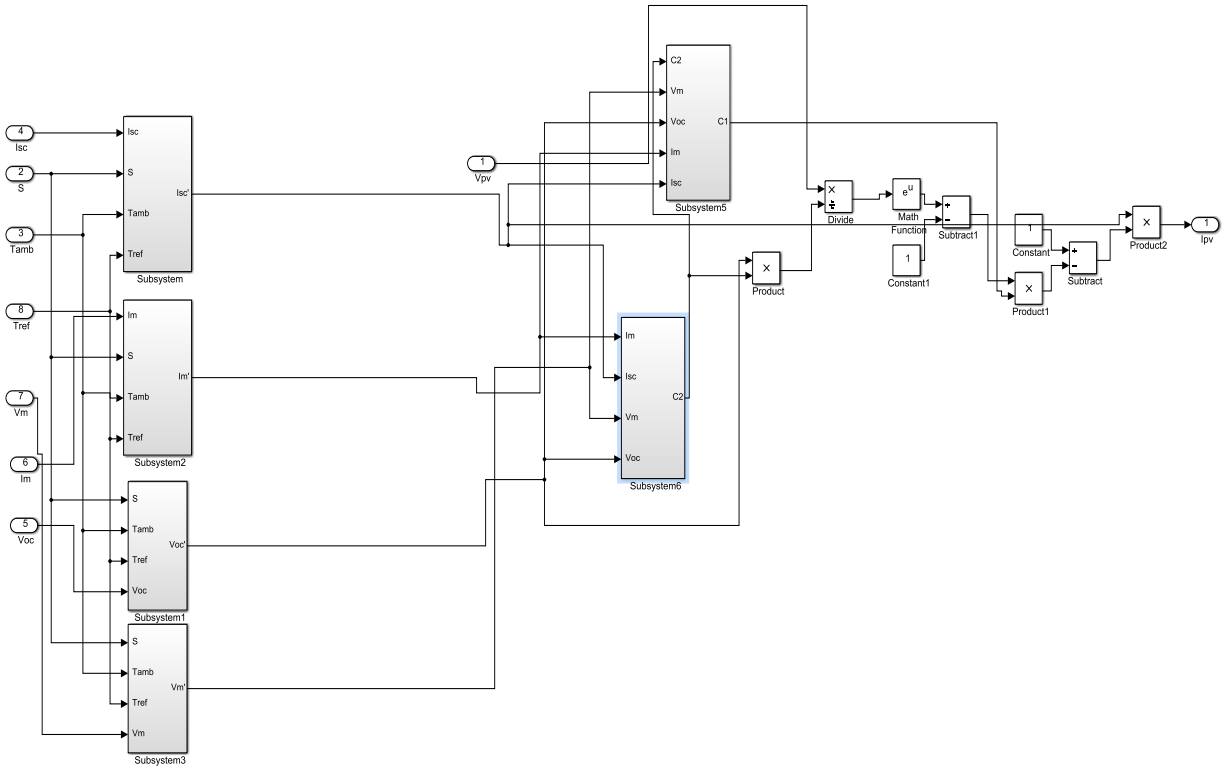

Figure 3.4 Simulink Model of Output of Photovoltaic Array

3.4.1.2 Simulink Photovoltaic Array Sub-System

Figure 3.5 shows the Simulink mask subsystem implementation of photovoltaic array. It was obtained from Figure 3.4 by combining the photovoltaic Simulink blocks into a sub system to reduce complexity.

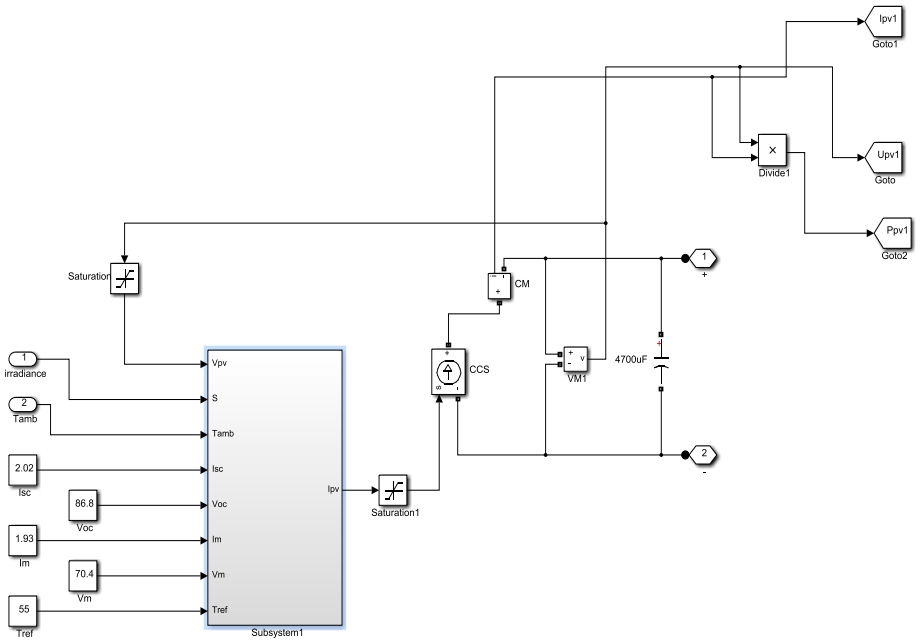

Figure 3.5: Photovoltaic Array Subsystem

The generated DC voltage of the photovoltaic panel is low for connection to the DC-link bus bar. Hence, the generated DC voltage level was increased using the DC-DC boost converter. The boost converter simply increases the output voltage of the photovoltaic system to a constant DC link voltage. The boost converter increases the photovoltaic DC voltage from 1400V to 3500V DC voltages.

3.4.2 Design of the Boost Converter

Current Ripple Factor (CRF): CRF selected as 10%.

i.e. $\frac{\Delta I_1}{I_1} = 10\%$

Voltage Ripple Factor (VRF): CRF selected as 5%

i.e. $\frac{V_o}{V_g} = 5\%$

Switching Frequency (f_s):f_s selected as 100KHz

10% and 5% were selected as values of CRF and VRF since according to International Electrotechnical Commission (IEC) harmonics standard, CRF and VRF should be bounded within 30%. So using smaller values for both the CRF and VRF will produce less ripples at the output voltage and current of the boost converter. Selecting 10% and 5% as values of CRF and VRF for the design will produce output with very minimal ripples hence no need to include filter in the design and the output can be connected to the output of the hydropower without filtering.

3.4.2.1 Design Specification:

In order to calculate the value of the capacitor, inductor and the duty cycle required in designing the boost converter the following specifications are used:

Input voltage, V_g= 1400V

Output voltage, V_o = 3500V

Output load current, I_o = 150A

V_g and V_o are selected as 1400V and 3500V because the boost converter input voltage is 1400V and output voltage of 3500V which is the input voltage required by the DC-AC inverter.

Calculation of Duty cycle (D):

$$\frac{V_o}{V_g} = \frac{1}{(1-D)} \tag{3.10}$$

$$\frac{1}{(1-D)} = \frac{3500}{1400}$$

D = 0.6

Calculation of Ripple Current (ΔI):

I_o = 150 A

ΔI_1= (0.1 * 150) A = 15A

Calculation of Inductor value (L):

$$L = \frac{V_g D}{f_s(\Delta I_L)} \tag{3.11}$$

L = (1400*0.6)/(15*100*10^3) = 0.56mH.

$$R_o = \frac{V_o}{I_o} = \frac{3500}{150} = 23.3333\Omega.$$

Calculation of capacitor value(C):

We have,

$$\frac{\Delta V_o}{V_o} = \frac{DT_s}{R_o C} \tag{3.12}$$

$$C = \frac{D}{Rf} * \frac{1}{\Delta V_o / V_o} \tag{3.13}$$

$$C = \frac{0.6}{23.3333 * 100 * 10^3 * 0.05} = 5.1429\mu F$$

The photovoltaic simulink model in Figure 3.5 was coupled with DC-DC boost converter to step the voltage from 1400V to 3500V as shown in Figure 3.6.

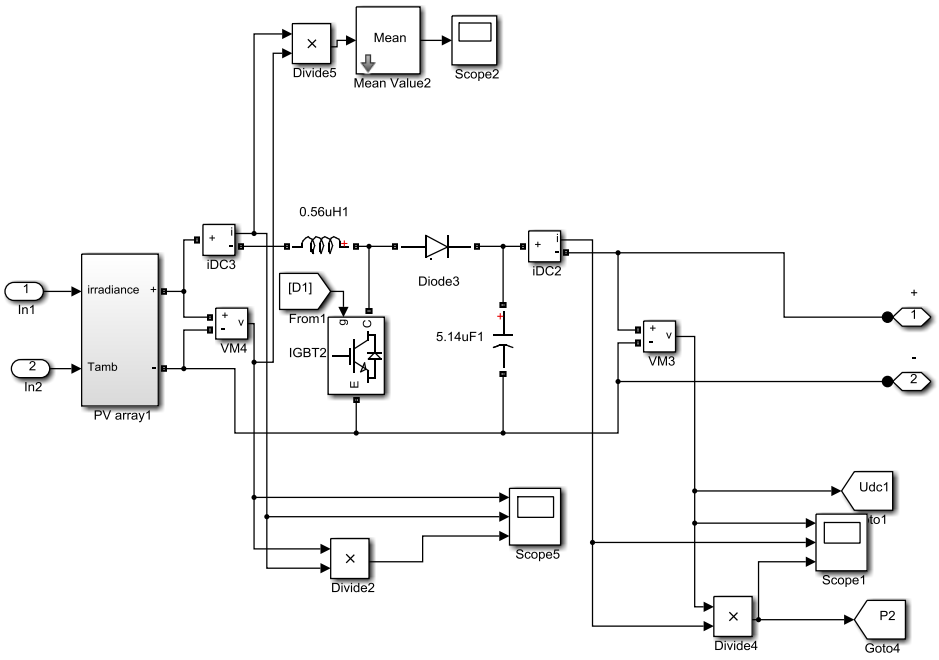

Figure 3.6: Simulink Model of the Photovoltaic Array with DC-DC Boost Converter

Figure 3.6 shows the photovoltaic array output connected to the input of the boost converter for the purpose of increasing the PV voltage from 1400V to 3500V DC voltage.

3.5 Model of Hydropower System

Power obtained from the solar system was 330kW while the deficit of power from the grid was 3.21MW from the result of load forecast. The hydro system therefore was design to produce 2.88MW. 1.5MW hydropower system is readily available and was used for hydropower generation system. Two hydro turbines that employed the use of 1.5MW reaction turbine coupled with self-excited induction generator (SEIG) were used for hydropower system development. The self-excited induction generator has the advantage of being an easy maintenance generator, rugged in construction, good self-protection against fault and readily available.

3.5.1. Hydropower Design

The design parameters for hydropower system are:

Discharge = 25.6 m^3/s

Head = 6.04m

Density of water = 1000kg/m^3

Acceleration due to gravity = 9.8m/s

Efficiency of the Turbine = 95%

The power generated by hydropower system is obtained using:

$$P_{hydro} = \eta_t \rho_w g q_w h_{util} \quad (2.14)$$

Since the system utilizes two hydropower turbines, the equation becomes:

$$P_{hydro} = 2\eta_t \rho_w g q_w h_{util} \quad (2.15)$$

$$P_{hydro} = 2(0.95 * 1000 * 9.8 * 25.6 * 6.04)$$

$$P_{hydro} = 2(1.44 * 10^6)$$

$$P_{hydro} = 2.88MW$$

The standard model for the turbine and generator model was used to develop the hydro system as highlighted in Figure 3.7

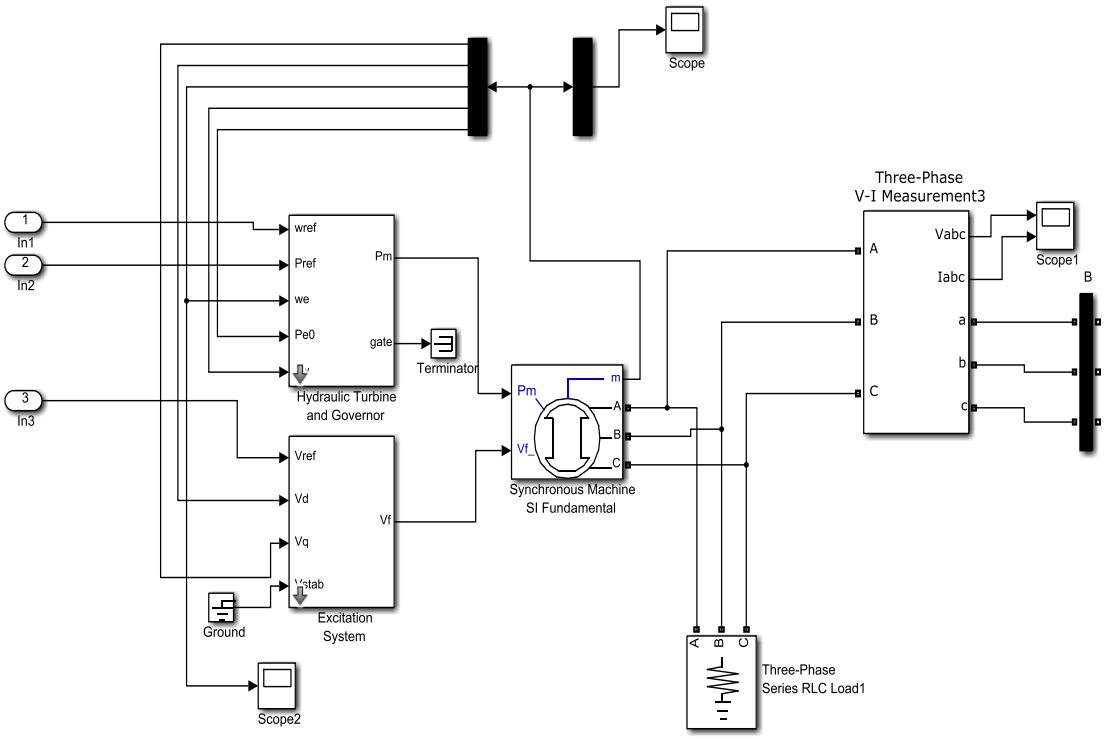

Figure 3.7: Simulink Model of the Hydropower System

To integrate the DC link of both hydro and solar power plant, the generated AC voltage of the hydro generator is converted into DC voltage. The AC voltage generated by self-excited induction generator is converted to the DC voltage using the universal bridge converter to 3500V. Simulink model of hydropower system with converter is shown in Figure 3.8

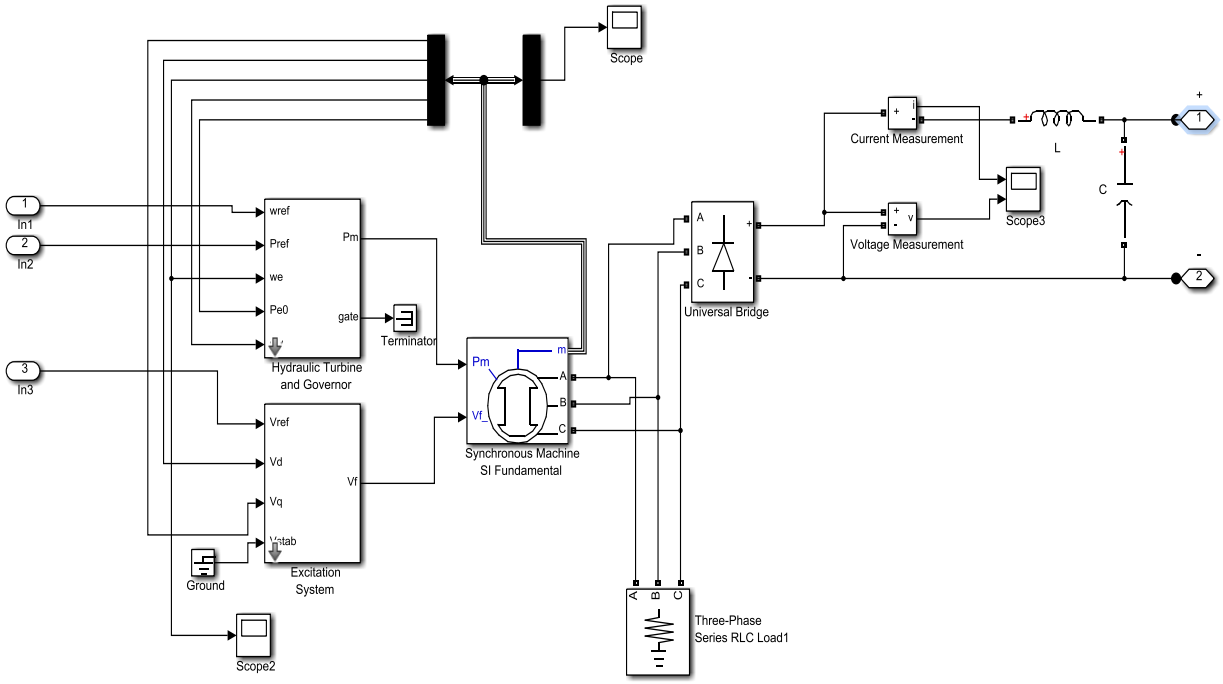

Figure 3.8: Simulation Model of Hydropower System with AC-DC Converter.

Figure 3.9 shows the mask hydropower subsystem Simulink model generated from Figure 3.8 by encapsulating the hydropower Simulink blocks into a subsystem block.

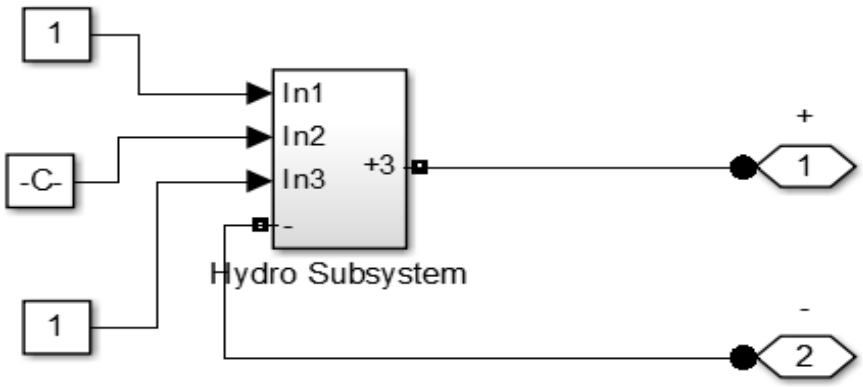

Figure 3.9: Mask Hydropower System

3.6 Model of Hybrid System

The Simulink model of the hybridization of the two primary sources was done which comprises of solar and hydro power systems. The DC link network topology was used and coupled to form

DC bus with 3500V DC voltage. The DC bus of the photovoltaic and hydro system has been common linked to reduce the cost and complexity of the hybrid system. Figure 3.10 shows parallel connection of the hydro and solar based hybrid power plant.

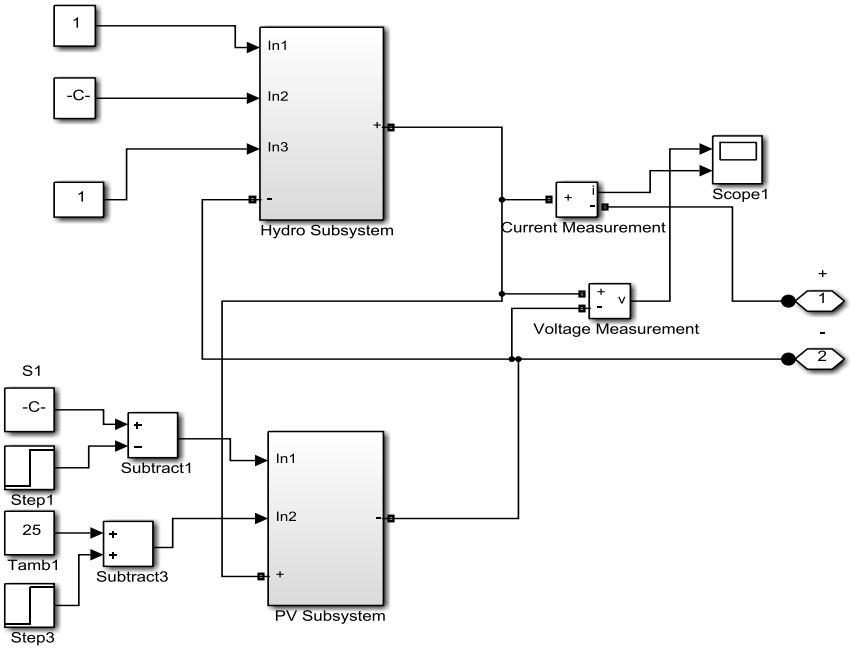

Figure 3.10: Hybrid Solar-Hydro Power System

A three phase universal bridge inverter was used to convert the DC voltage to three phase AC voltage. Universal bridge inverter was used because it is very versatile and can be used for both DC-DC and DC-AC conversion. Universal bridge converter can also be implemented in full-bridge form with two switching legs or in half-bridge form with one switching leg.

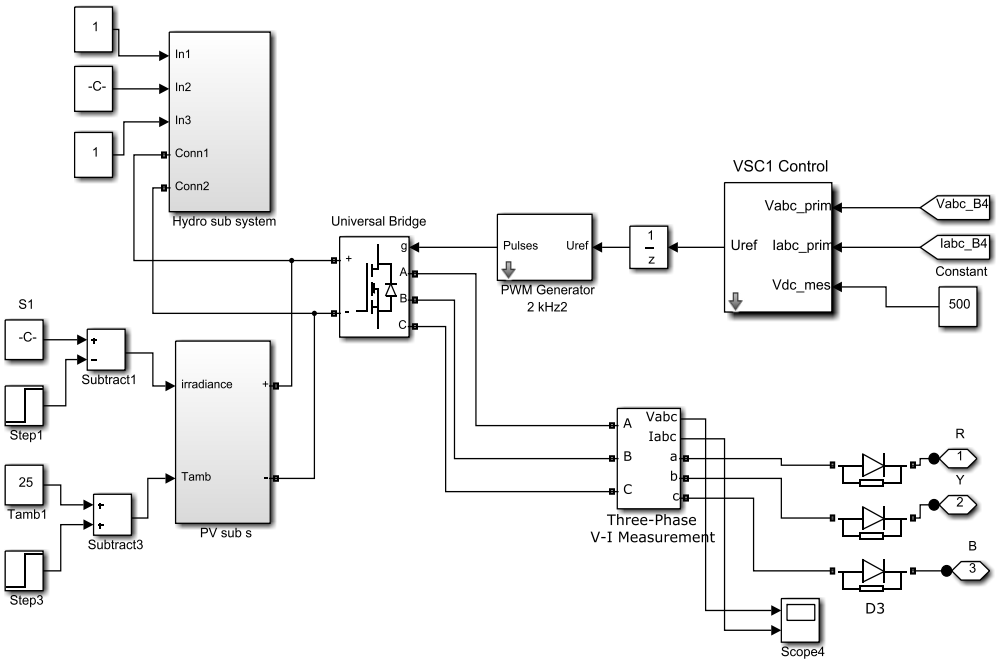

Figure 3.11: Hybrid Solar-Hydro System Coupled with DC-AC inverter

Step up transformer was used to step the inverter output voltage to 33kV. Beside this, it provides isolation and prevents injection of DC current into the grid. A phase lock loop (PLL) was developed to synchronize the system output with the grid.

3.6.1 Design of Phase Locked Loop

The phase locked loop was used to synchronize the hybrid system with the grid. Phase locked loop was used because it provides fast and accurate synchronization information with a high degree of immunity and insensitivity to disturbances, harmonics, unbalances, sags/swells, notches and other types of disturbances in the input signal (Padua, 2005).The Grid voltages V_a, V_b and V_c are transformed from three phases to a stationary system of two phases Vα and Vβ using equation (2.42) and from Vα-β to V_{d-q}. The Simulink transformation model of abc-αβ and αβ-dq is shown in Figure 3.12 and 3.13.

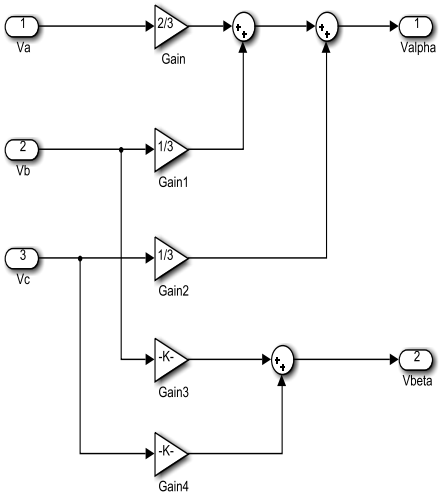

Figure 3.12: Transformation from abc-αβ

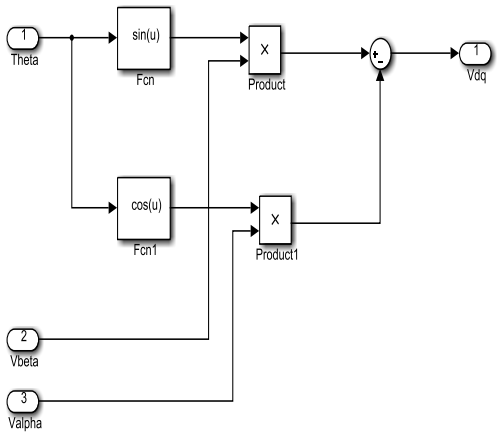

Figure 3.13: Transformation from αβ-dq

Selecting the root mean square of the line-to-line voltage to be 33kV at the point of grid connection, the amplitude voltage level, Vm is calculated as:

$$V_m = \frac{\sqrt{2}}{\sqrt{3}} * 33000 = 26.944kV \tag{3.16}$$

Frequency of the utility grid selected as 50Hz

Line-to-line voltage was selected to be 33kV because the hybrid system will be coupled to 33kV side of the grid while 50Hz frequency was selected because the grid frequency is 50Hz.

The design parameters are therefore as follows:

$V = 26.944kV,$ $T_s = \frac{1}{f} = \frac{1}{5000s} = 0.2ms,$ Crossover Frequency, $f_c = 50\ Hz$

$\omega_c = 2\pi f_c rad/s = 314.3\ rad/s$

Substituting the design parameters into equation (2.59) gives:

$$\begin{cases} a = 16 \\ \tau = 0.05 \\ K_p = 0.0116 \end{cases} \tag{3.17}$$

From the PI regulator function in equation (2.55), the transfer function with gain in s-domain was obtained as:

$$G_{pi} = kp\frac{1+S\tau}{S\tau} = \frac{0.00058s+0.0116}{0.05s} \tag{3.18}$$

The implementation of the PI regulator in Simulink is as shown in Figure 3.14

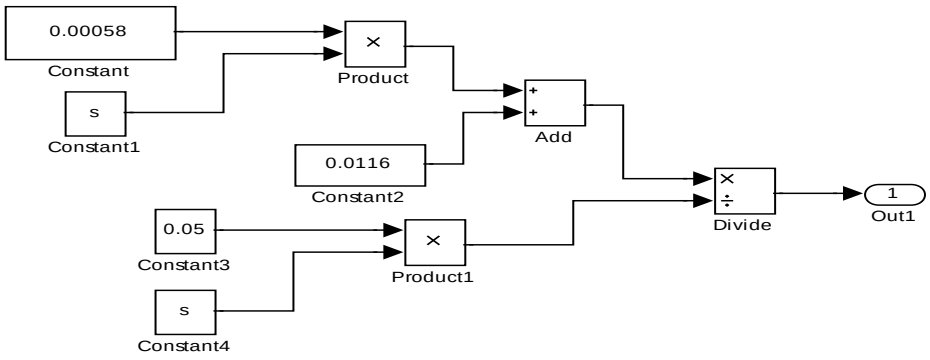

Figure 3.14: PI-Regulator Simulink Implementation

The filter transfer function was obtained from the transfer function of the PLL (given in equation 2.44) by putting parameter values of equation (3.17) into the filter transfer function, we obtained equation (3.19)

$$G_{filter} = \frac{1}{1+STs} = \frac{1}{0.0002s+1} \tag{3.19}$$

The Simulink implementation of the filter is as shown in Figure (3.15)

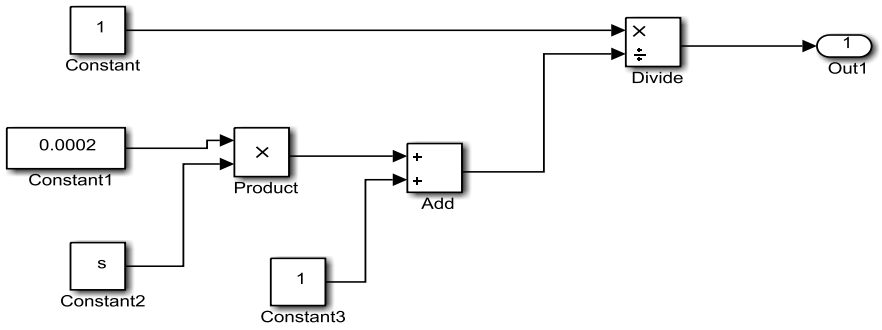

Figure 3.15: Simulink Implementation of Filter

Using the values of equation (3.17), into equation (2.45) gives the transfer function for the open loop system as:

$$G_{ol} = \left(kp\,\frac{1+S\tau}{S\tau}\right)\left(\frac{1}{1+STs}\right)\left(\frac{V_m}{s}\right) = \frac{15.6275s+312.55}{0.00001s^3+0.05s^2}, \tag{3.20}$$

The resulting configuration of phase lock loop is as shown in Figure (3.16)

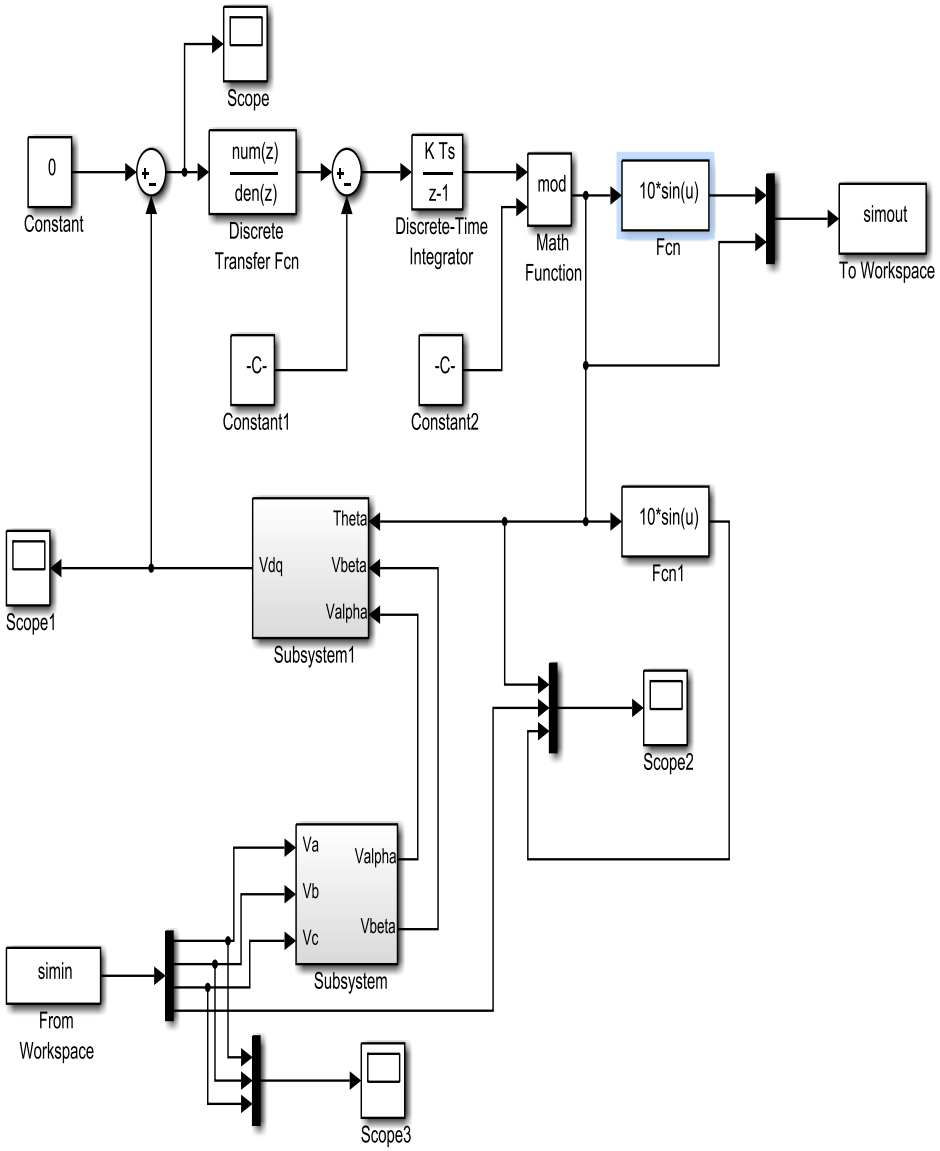

Figure 3.16: The Simulink Model of the Phase Lock Loop System

3.7 Model of Cascaded System

This model includes the photovoltaic module, hydro module, grid, transformers, converters, inverter and other measuring devices.

Figure 3.17 shows the Simulink model for the entire grid integrated hybrid systems

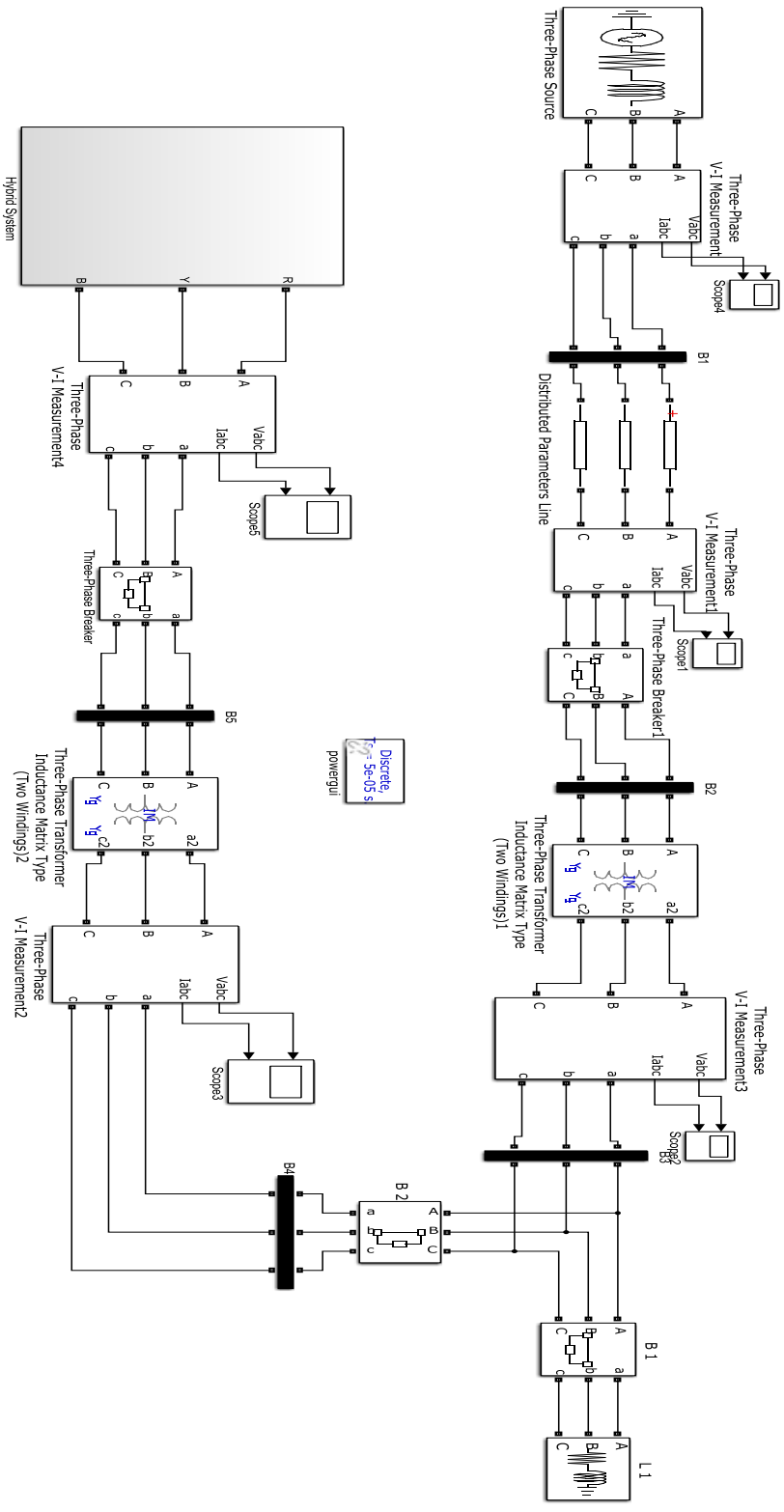

Figure 3.17 Cascaded Simulink Model of the Grid Connected Hybrid System.

CHAPTER FOUR

RESULTS AND DISCUSSION

4.1 Introduction

This chapter summarizes the detailed result obtained for the hybrid system and load profiling model.

4.2Result of Load Profiling

Load profiling was done using artificial neural network based on Bayesian regularization algorithm so as to determine the future power demand of the area under study. A code was developed as shown in Appendix A that utilizes Bayesian regularization algorithm using artificial neural network technique for the load forecasting. Three years load demand data obtained from TCN and three years weather condition data obtained from NIMET were shared into three sets of data 40% of the data as first set, 30% as second set and 30% as the third set. First and second were used for training and testing respectively while the third set was used for validation. This data's were then used to forecast the future load demand and was compared with the present demand. The result is as shown in Table 4.1.

Table 4.1: Actual Demand and Next Year Load Demand

Month	Actual Demand (MW)	Next Year (MW)
1	12.39	16.87
2	15.62	16.53
3	17.18	18.29
4	16.62	17.02
5	17.54	18.73
6	17	16.27
7	17.92	19.68
8	19.39	19.98
9	20.55	18.21
10	19.35	19.83
11	18.47	14.97
12	19.38	18.24
Total	211.41	214.62

The load profiling was carried out and the deficit power was obtained. Table 4.1 shows the total load demand for the present year 211.41MW as against 214.62MW for the next year forecast. This result shows that 3.21MW deficit of power was obtained from the grid which could be due to network expansion and constant allocation of same power from the utility to the consumers and this brought the need to augment the power from the grid using solar-hydro hybrid system. The hybrid system was developed that will not only carter for the deficit but also improve the power quantity and security of the grid.

4.3 Result Based on Hybrid System

The result of the network behavior of the solar-hydro hybrid grid connected system was obtained and presented. The result comprises the hydropower system, solar photovoltaic system and hybrid system results.

4.3.1 Hydropower System

Two hydro turbines that employed the use of 1.5MW reaction turbine coupled with self-excited induction generator (SEIG) were used for hydropower system development. Figure 4.1 shows the generated AC voltage, current and power of the self-excited induction generator.

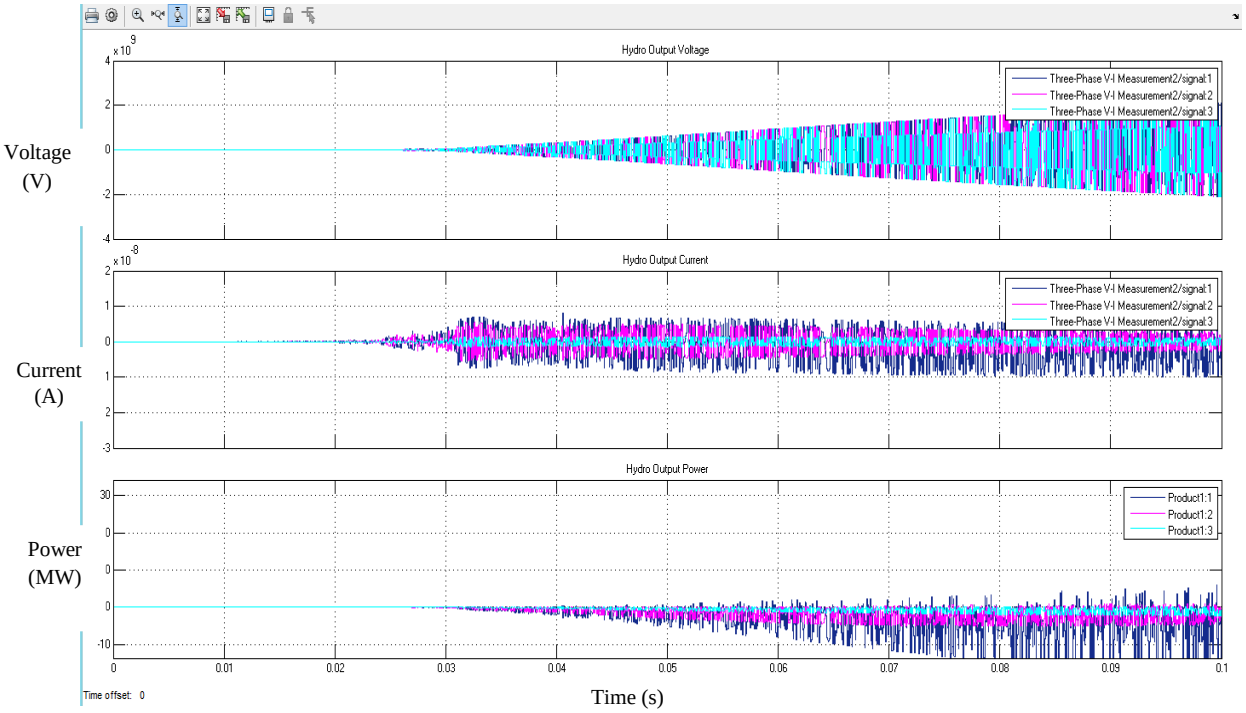

Figure 4.1: Output Voltage, Current and Power of the Self-Excited Induction Generator

The output of the hydro generator voltage, current and power have a sinusoidal waveform as shown in Figure 4.1. To integrate the DC link of both the hydro and solar power plant, the generated AC voltage of the self-excited induction generator is converted into DC voltage via diode rectifier (Figure 3.8). The DC output of the diode rectifier is as shown in Figure 4.2.

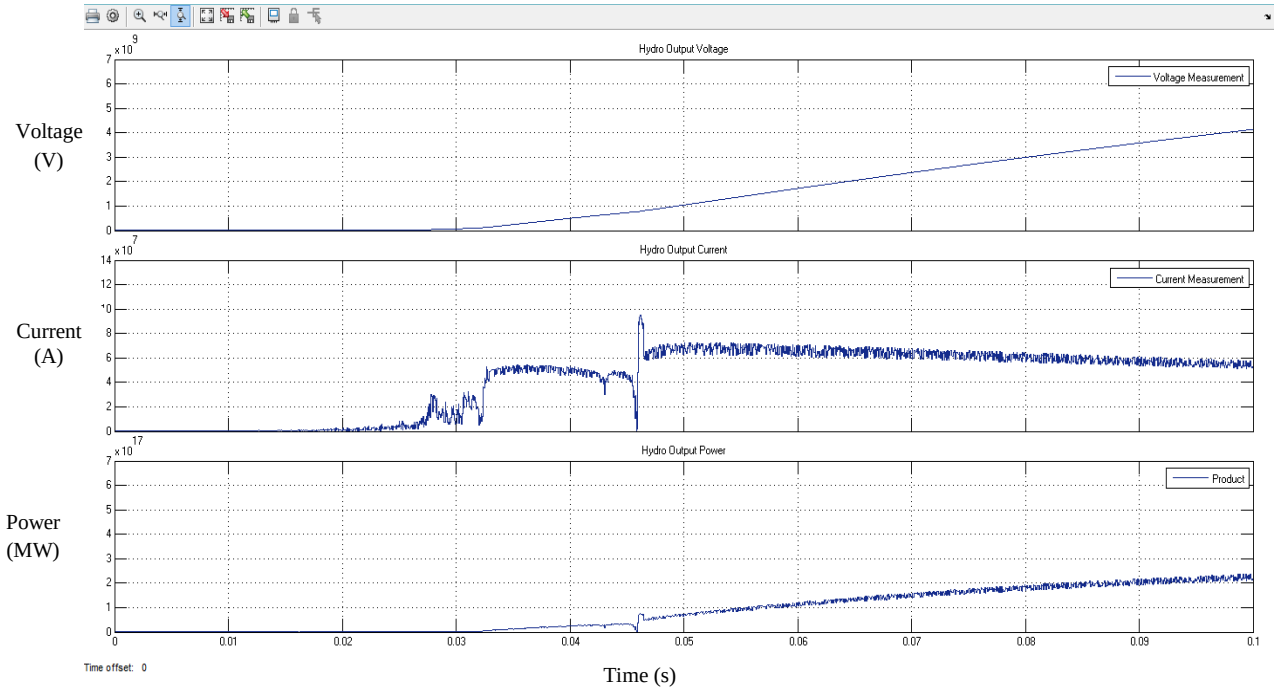

Figure 4.2: Output Voltage, Current and Power Waveform of Hydro Converter

The output AC voltage and current from the hydro system was converted to DC voltage using the diode rectifier as shown in Figure 4.2. The current waveform was unstable at about 0.04 seconds to 0.05 seconds and that can be as a result of excitation current generated by the self-excited generator.

4.3.2 Solar Photovoltaic System

The solar PV system adopted the use of Solarex MSX64 using average solar radiation intensity of 653.45W/m^2. Figure 4.3 shows the variation in solar irradiance and voltage, current and power generated by the photovoltaic system at the variable solar irradiance before boost converter.

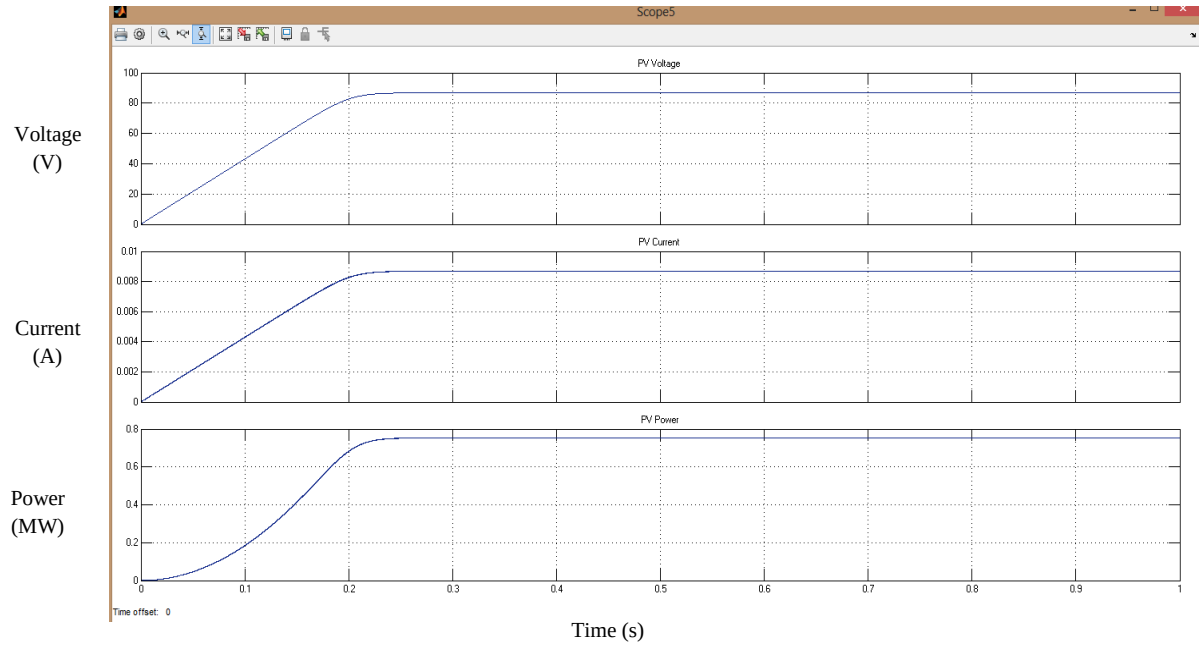

Figure 4.3 Solar Photovoltaic Module Output

Figure 4.3: Shows that the solar photovoltaic system output voltage was a DC voltage. The solar photovoltaic system output voltage and current starts from zero which corresponds to morning when there is no solar radiation. The output of the solar photovoltaic system begins at zero point which corresponds to morning as shown in Figure 4.3. The PV array output voltage generated was low for integrating to the DC link of the power plant. Hence, DC-DC boost converter was used for enhancing the voltage level (Figure 3.6) to 3500Vas shown in Figure 4.4.

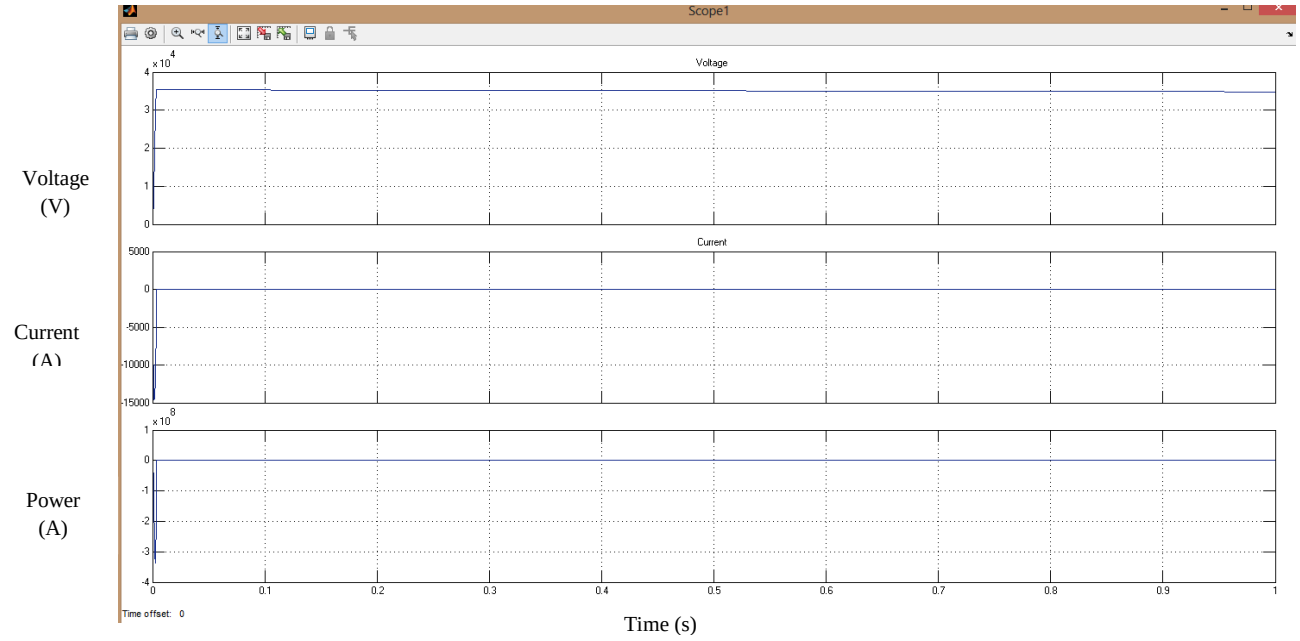

Figure 4.4: Output of Photovoltaic Boost Converter

The boost converter was used to increase the DC voltage of the solar photovoltaic system to a higher value (3500V) as shown in Figure 4.4. This voltage corresponds to the DC voltage of the DC bus bar and also corresponds to the DC voltage output from the diode rectifier of the hydro system. The DC link voltage of both the solar photovoltaic and hydropower plants are coupled to form DC bus with 3500V DC voltage as shown in Figure 4.5.

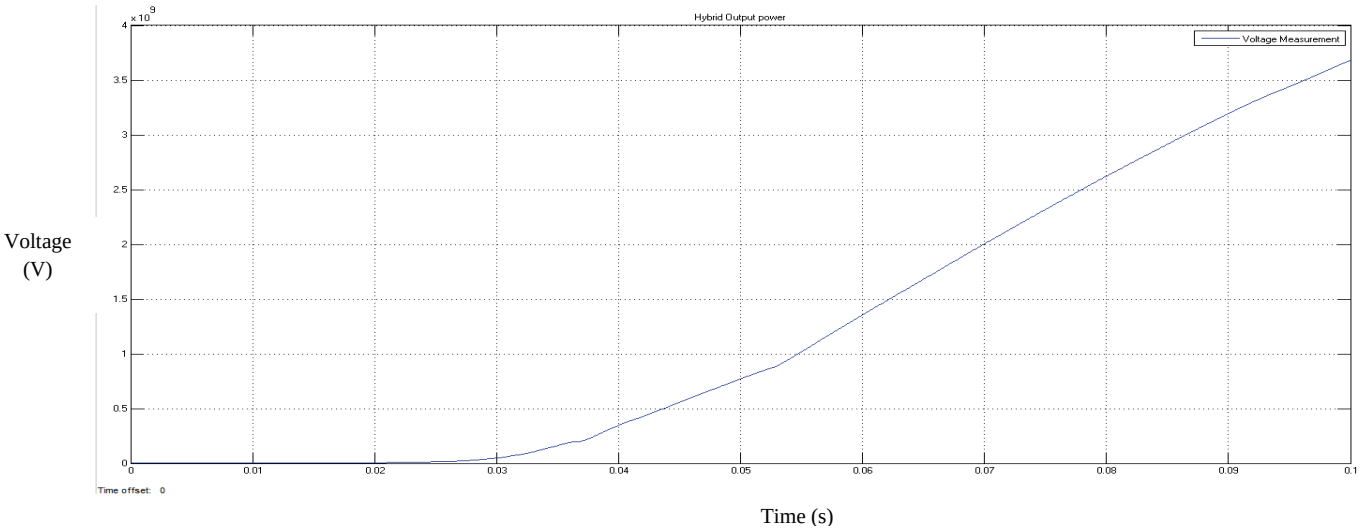

Figure 4.5: Hybrid Output Voltage

Figure 4.5 shows the generated voltage from hydro and solar based hybrid power plant. The voltage of the hybrid solar-hydro hybrid system was 3500 DC voltage as shown in Figure 4.5.

To integrate grid with the hybrid energy systems, DC output voltage from the hybrid system was converted into pure sinusoidal AC voltage using DC-AC inverter (Figure 3.11). Figure 4.6 shows the inverter AC output voltage and current.

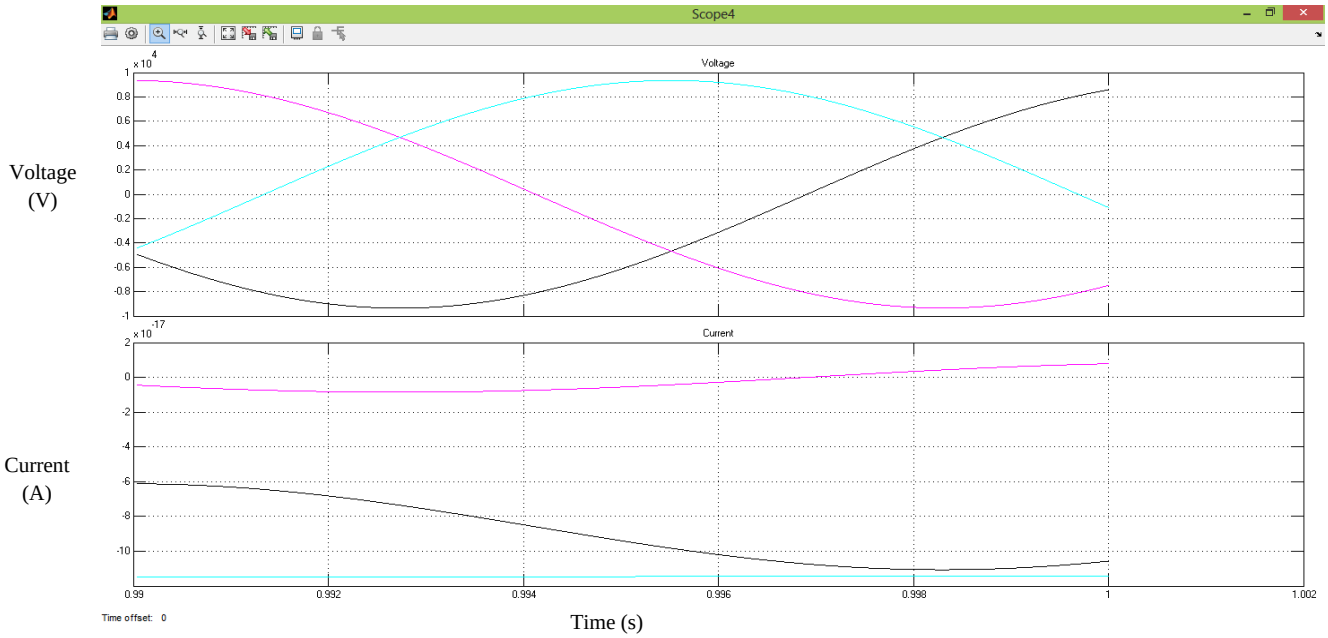

Figure 4.6: Inverter Output of the Hybrid System

The inverter AC voltage and current waveform is as shown in Figure 4.6. From Figure 4.6, the voltage and current waveform was sinusoidal. The output voltage of the inverter was less than the grid voltage. To connect the hybrid power plants in parallel with the 132kV 150MVA utility grid, the voltage level must be the same. Hence a step-up transformer increases the voltage level of the interfacing inverter to 33kV and a step-down transformer decreasing the voltage level of the grid voltage from 132kV to 33kV. The output of the transformer which is the output of the entire system consisting of the solar-hydro hybrid system before connecting to grid is shown in Figure 4.7

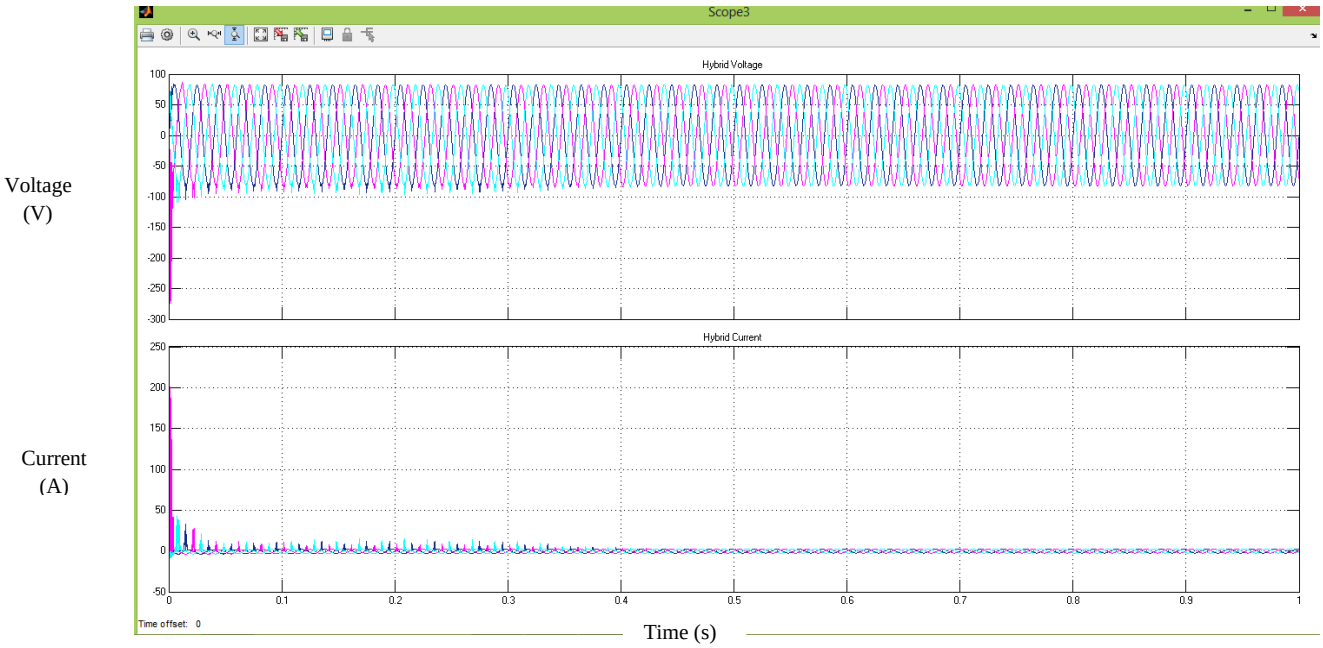

Figure 4.7 Waveform of Voltage and Current of the Hybrid System

Figure 4.7 shows that the step-up transformer output voltage and current waveforms. The inverter output was step-up to the grid voltage using the step-up transformer to enable connecting the hybrid system to the grid. The step-up transformer produces a pure sinusoidal output which prevents injecting ripples into the grid. The transformer stepped the inverter output voltage to 33kV to enable synchronization with the grid as shown in Figure 4.7.The output of the hybrid system was injected to the grid at 33kV side of the utility grid with a load of 18.24MW via a phase lock loop. The phase locked loop was used to synchronize the hybrid system to the grid for synchronous operation of the entire system. The 132kV output of the grid is shown in Figure 4.8.

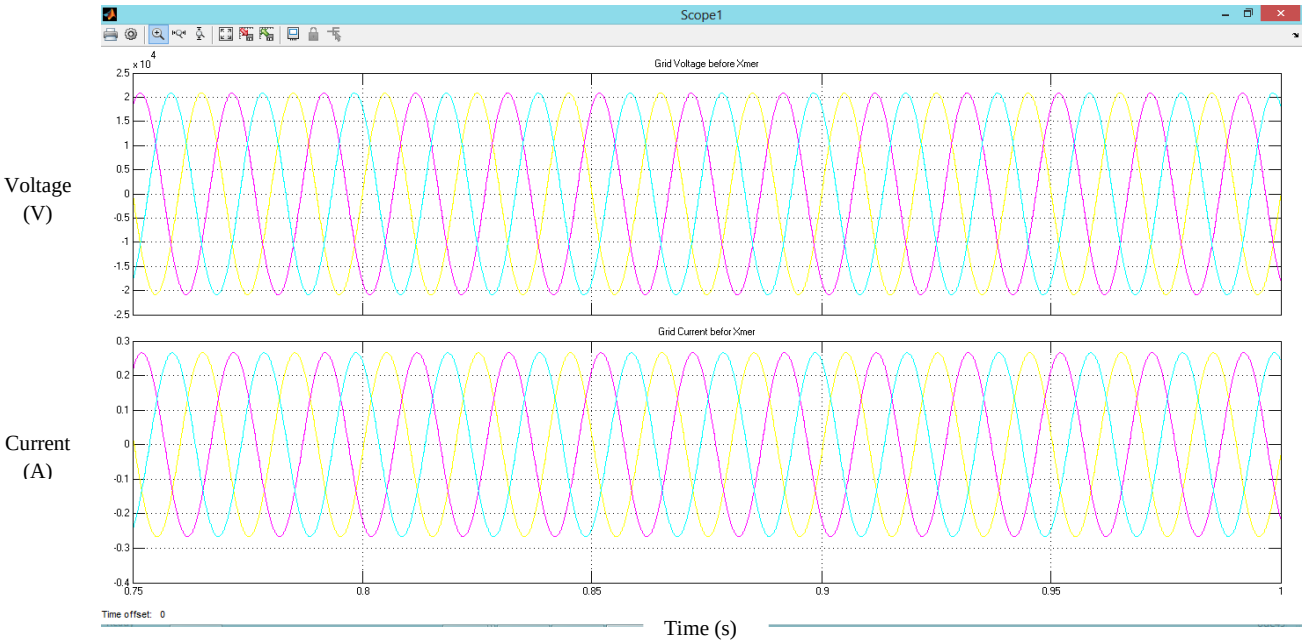

Figure 4.8: 132kV Voltage of the Utility

The voltage from the solar-hydro hybrid system output was 33kV as shown in Figure 4.7, hence the 132kV side of the utility was step down using step-down transformer to 33kV which is equivalent output voltage of the hybrid power system developed. The 33kV output of the utility grid before connecting the hybrid system and the load is as shown in Figure 4.9.

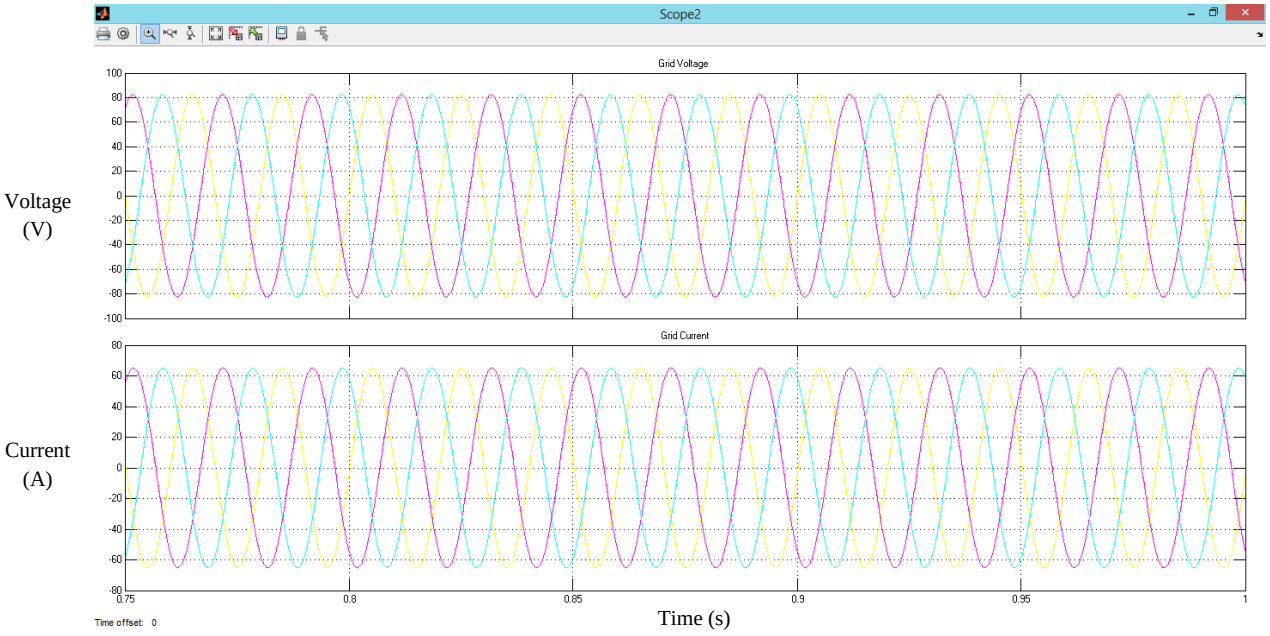

Figure 4.9: Output of the 33kV Side of Utility Grid before Connecting Grid and Load

The step-down transformer has step down the grid voltage to 33kV as shown in Figure 4.9.The 33kV side of the utility grid have same voltage with the output voltage obtained from the hybrid system hence the rest of the parameters and control was done by the phase lock loop used for synchronizing the grid with the hybrid system. Figure 4.10 shows the voltage and current waveform of the grid after synchronizing with hybrid system with a load of 18.24MW.

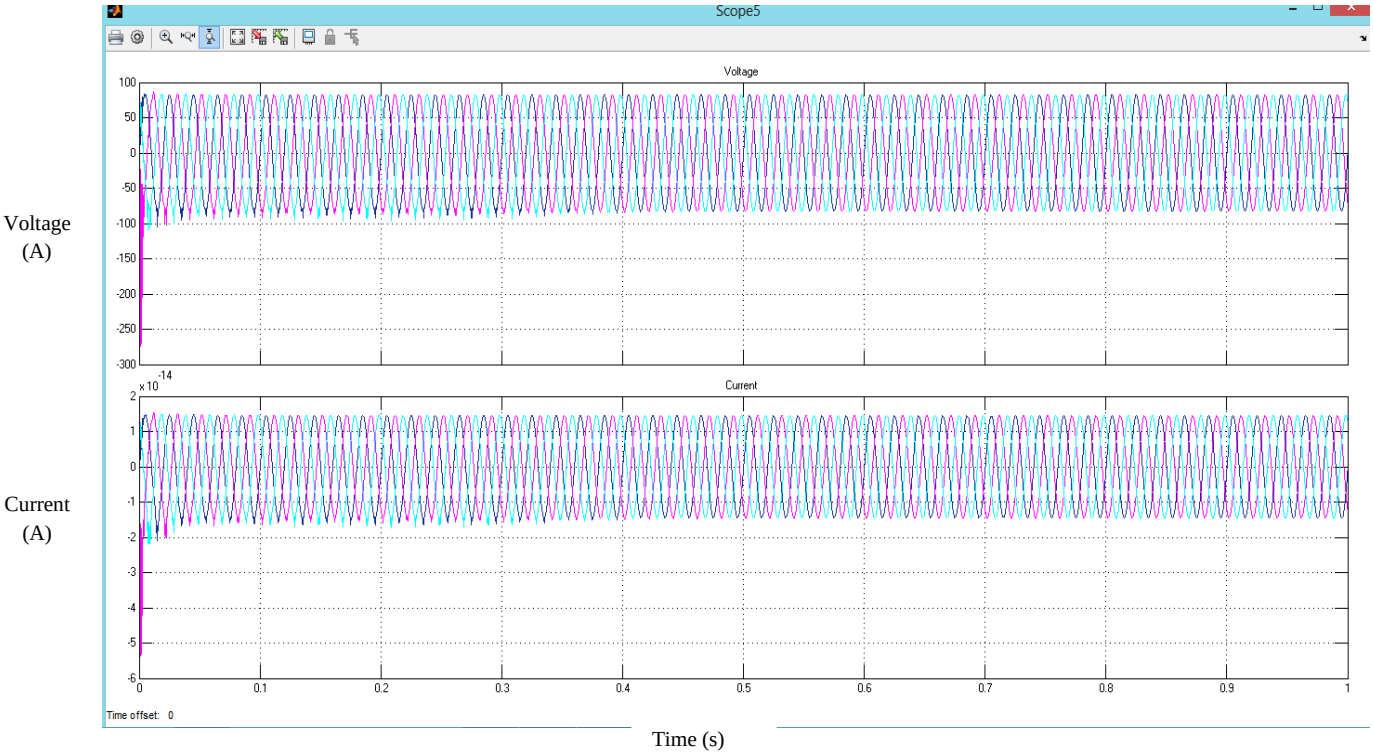

Figure 4.10: Output of Grid Connected, Load and Hybrid System

Figure 4.10 shows that the voltage waveform of the utility and that of the hybrid system remains the same after synchronization. This shows that the hybrid output voltage was the same with the grid voltage(33kV). The output power obtained from the hybrid system, the grid and the grid connected hybrid system is as shown in Figure 4.11.

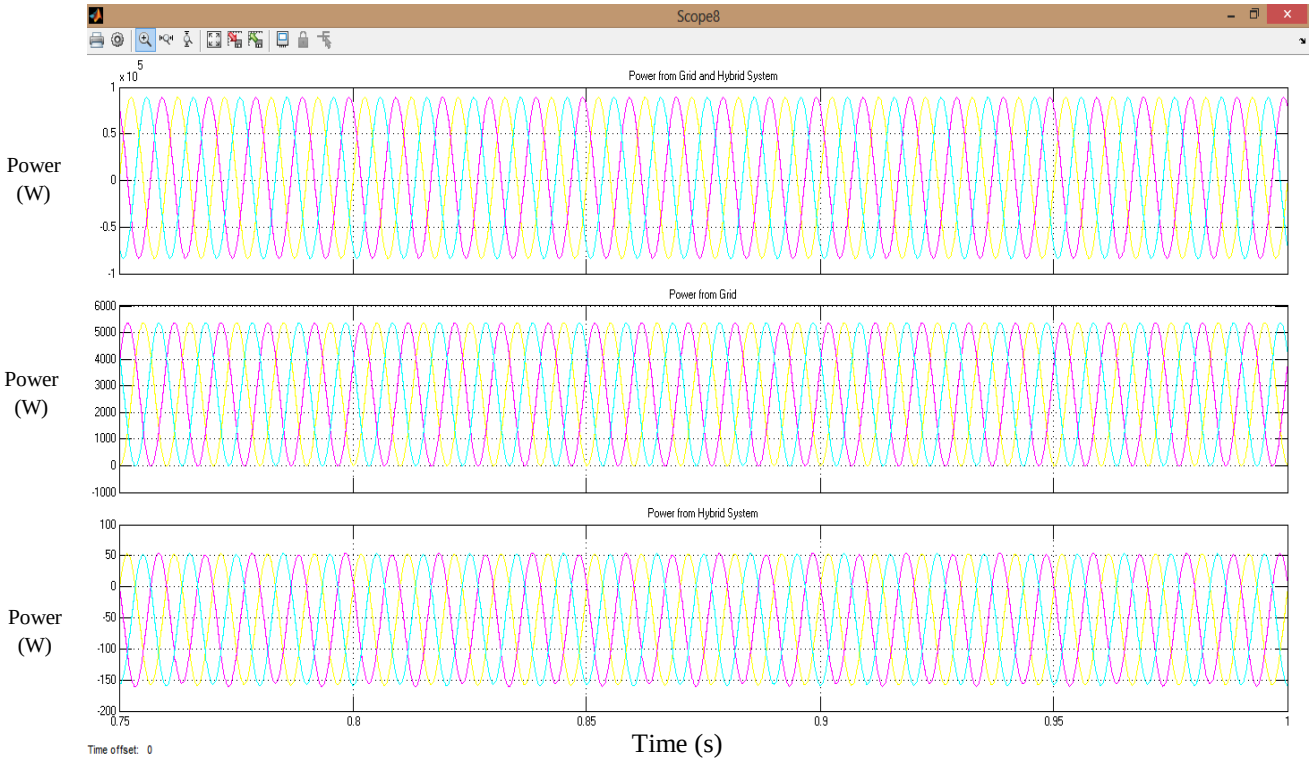

Figure 4.11: Power from the Grid Connected Hybrid System, Grid and Hybrid System

Figure 4.11 shows that the power obtained from the grid before connecting with the hybrid system was increased by 3.21 MW after connecting the hybrid system and load. This implies that the developed hybrid system was able to augment the deficit of power from the grid. This system also enhances the grid power quantity, reliability and security.

4.4 Validation

The developed model results was validated using meshram model and the result of meshram model compared with the developed model is as shown in Figure 4.12 to 4.10.

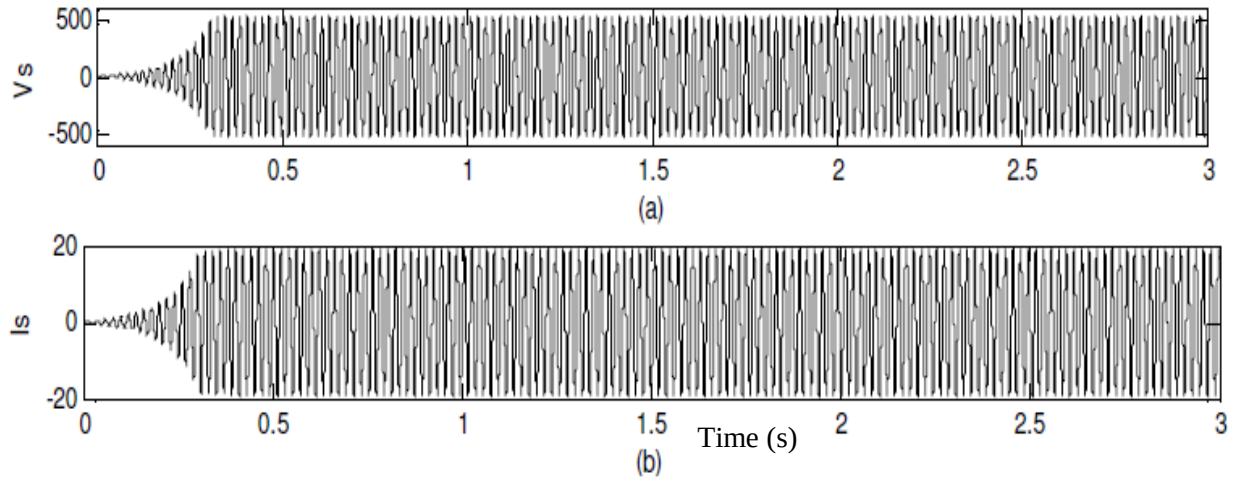

Figure 4.12: Output Voltage and Current of the SEIG

Figure 4.12(a) and (b) shows the generated AC voltage and current of the SEIG which is in conformity with Figure 4.1 obtained from the developed model.

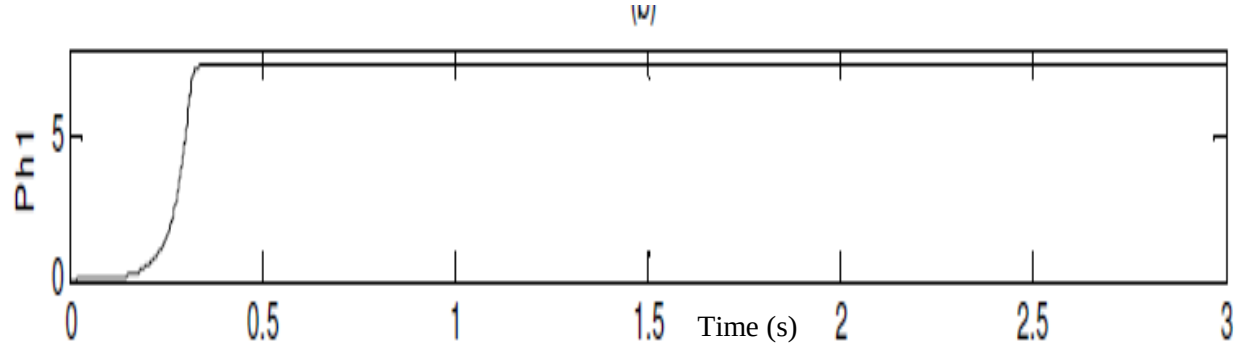

Figure 4.13: Output Power of the Hydro SEIG System

Figure 4.13 shows the generated power of the SEIG system after rectification which is in conformity with Figure 4.2.

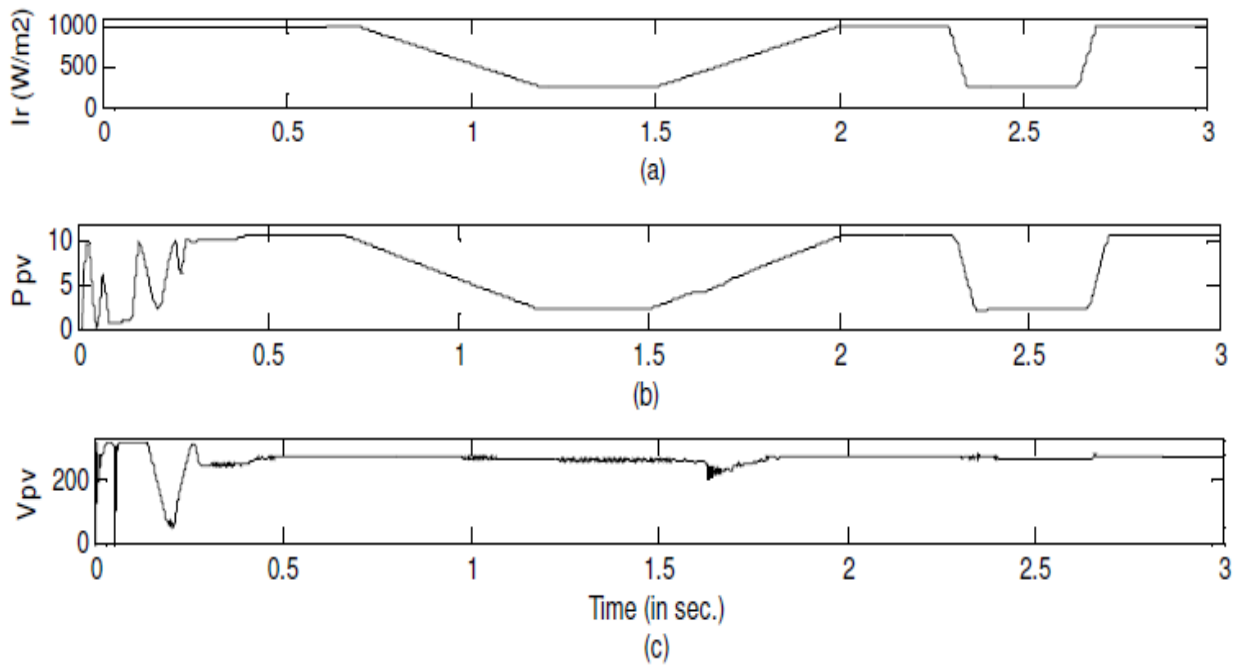

Figure 4.14: Generated DC Voltage, Current and Power of the PV Array

Figure 4.14 shows the output voltage, current and power generated from the PV module at the variable solar irradiance in the meshram model. The waveform is in conformity with the output voltage, current and power from the developed model (Figure 4.4) but this was taking for a longer period of time as compared to the developed model output (Figure 4.4).

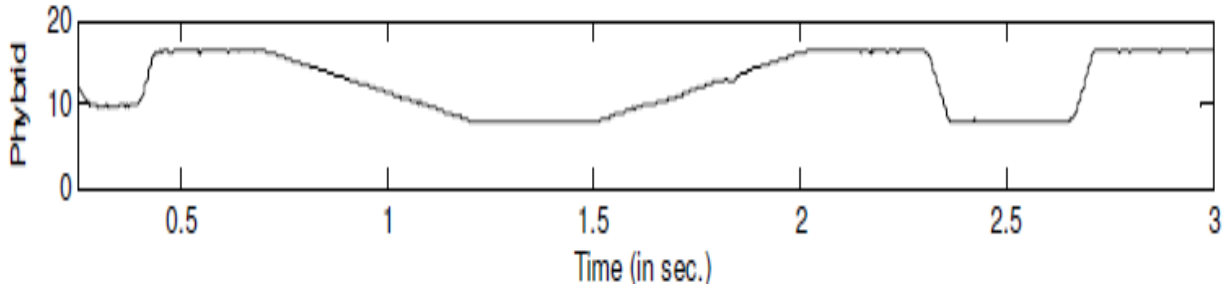

Figure 4.15: Generated Power with the PV/Hydro Hybrid System

Figure 4.15 shows the generation of power by the hydro and solar based hybrid power plant with the variation in solar irradiation which conforms with Figure 4.5.

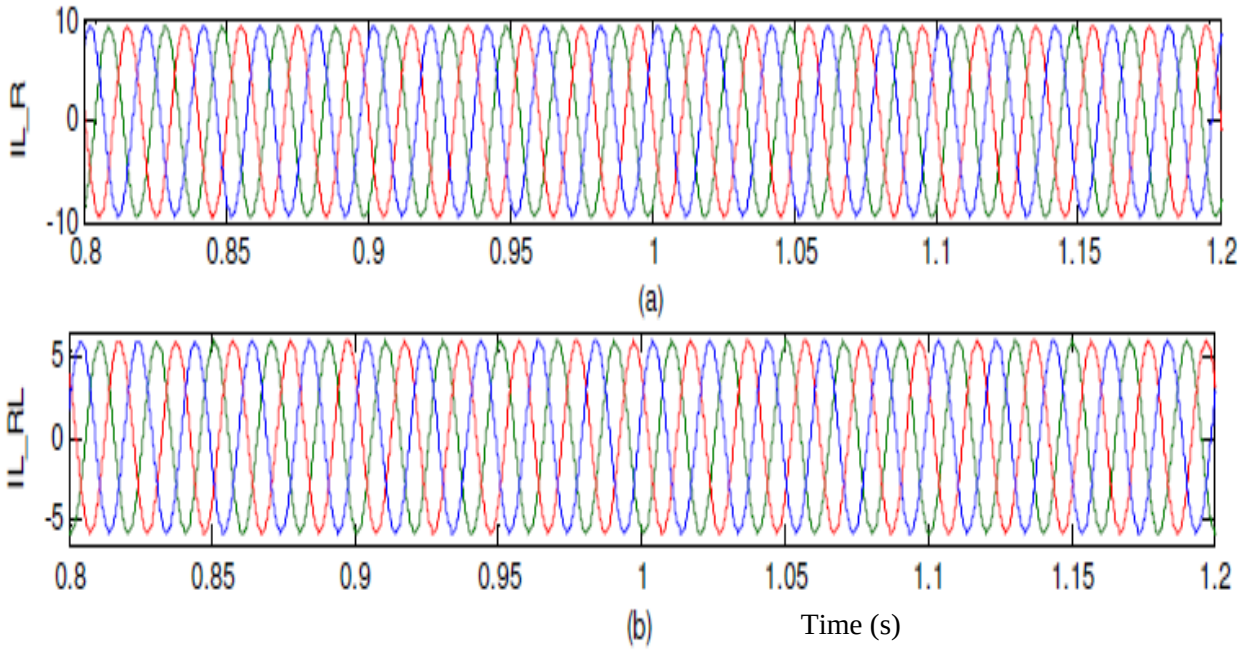

Figure 4.16: Output of the Hybrid System

Figure 4.16 shows the waveform of load current for the resistive and resistive inductive load and both are in conformity with the output of the grid connected, load and hybrid system output waveform of Figure 4.10.

These results show that the developed approach is in conformity with meshram and other algorithms.

4.5 Discussion of Results

An artificial neural network model was developed based on Bayesian regularization algorithm considering environmental conditions (temperature, relative humidity, rainfall, wind speed, solar radiation and sunshine hours). The one year forecasted result of the model when compared with the current load demand obtained from utility, a deficit of 3.21MW power was obtained. This deficit power was taken care of by developing a hydro-solar hybrid system where the hydropower system produced 2.88MW and the solar photovoltaic system produced 330kW. The hybrid system was able to supplement a total power of 3.21MW to the grid using two hydro turbines that employed the use of 1.5MW reaction turbine coupled with self-excited induction generator for hydropower system development and Solarex MSX64 photovoltaic array for the solar photovoltaic generation system. The AC voltage of the hydro system was converted to DC to enable connection to solar PV system. The solar system output voltage was low and a boost converter was used to increase the solar system output voltage before connected with the hydro system. The DC voltage of the hybrid system was converted into AC voltage using universal bridge inverter and step-up transformer steps the voltage to 33kV. The solar-hydro system was integrated into the 33kV side of the utility. A 30MVA, 132 kV/33 kV step-down transformer was used for bringing the AC voltage level of the utility to the level of solar-hydro hybrid system voltage (33kV).

CHAPTER FIVE

CONCLUSION AND RECOMMENDATIONS

5.1 Introduction

This chapter presents conclusion based on the discussion of the results obtained in chapter four and summary of the work done. Recommendations for further work and some of the limitations encountered are also presented.

5.2 Conclusion

In this work, a load forecasting model was developed using artificial neural network and implemented on a Matlab R2013b environment. The implementation of the network architecture, training of the neural network and simulation of test results were achieved based on Bayesian regularization training algorithm. The model was developed considering load demand, temperature, relative humidity, rainfall, wind speed, solar radiation and sunshine. The load profiling was carried out and deficit power of 3.21MW was obtained which brought the need to augment the power from the grid using solar-hydro hybrid system. This deficit of power supply from the grid observed was taken care of by developing a grid connected solar-hydro hybrid system model. The simulation modeling and performance analysis of the grid connected DC-linked solar-hydro hybrid system was done using MATLAB/Simulink toolbox. The system works to compensate the deficit power found in power grid, Based on the result obtained from the developed hybrid system, the hydropower system produced 2.88MW and the solar photovoltaic system produced 330kW. The hybrid system was able to supplement a total power of 3.21MW to the grid. The results obtained show that the developed hybrid system can supplement the deficit electric power to the grid efficiently.

5.3 Recommendation for Further Work

Future work should consider the following area of research for the advancement of this work:

1. The system can be designed in such a way that it can detect islanding and take necessary action/decision.

2. The grid connected solar-hydro hybrid system should be extended to consider a standalone mode of operation that will supply part of Kaduna north when grid is not available

3. Adding other renewable energy sources such as wind turbine to the hybrid system should also be considered.

4. Incorporating storage means as part of the system is another section that can be considered as recommendation for future work in this field.

5.4 Significant Contributions

This research work offers the following significant contributions to the existing body of knowledge:

1. Development of a solar-hydro hybrid power generation Simulink model capable of generating 3.21MW to supplement power supply to the grid and capable of supporting the utility network in terms of improving the power quantity and security;

2. Integrating and synchronizing the solar-hydro hybrid system to the grid using Phase Locked Loop;

3. Development of a load forecasting model using Artificial Neural Network based on Bayesian regularization algorithm putting in cognizance the previous load demand data and other

environmental conditions (Temperature, relative humidity, rainfall, wind speed, solar radiation and sunshine hours).

5.5 Limitations

During the course of this work, certain limitations were observed which are itemized as follows:

1. The scope of this work was limited to the case where power from the grid is available hence the effect of power failure or black out from the grid was not captured.

2. The dynamic nature of load in a typical sub-transmission network was not considered.

3. All protective devices are assumed to be fully coordinated.

REFERENCES

Abacha, H.G., Ahmad M.Y.J., & Ladan, M. (2011). Design and Simulation of a Hybrid PV/Fuel Cell Energy System. *Continental J. Engineering Science,* 6 (1), 37- 45.

Abu-Jasser, A. (2010). A Stand-alone photovoltaic system, case study: A residence in Gaza', *Jour-nal of Applied Sciences in Environmental Sanitation,* 5(1): 81-91

Aleksandr, C. (2009). Use of Artificial Neural Networks for Short Term Electricity Load Forecasting of Kenya National Grid Power System. *International Journal of Computer Applications,* 0975-8887, 63(2) 25-30

Arun, S., & Dilip, D. (2012). Optimised Hybrid Integrated Renewable Energy System. *An International Journal of Advanced Computer Technology,*1(1) 1-8.

Aslan, Y., Yavasca, S., & Yasar, C. (2011). Long Term Electric Peak Load Forecasting of Kutahya using Different Approaches. *International Journal on Technical and Physical Problems of Engineering,*(IJTPE), ISSN 2077-3528, 87-91.

Badran, S. M., & Abouelatta, B. O. (2013). Forecasting Electrical Load Using Artificial Neural Network combined with Multiple Regression Method. *The Research Bulletin of Jordan,* ACM, 11 (11) 52-58.

Basaran, U. F., Nezih, O. G., & Kurban, M. (2011). Hourly forecasting of Long Term Electric Energy Demand Using Noval Mathematical Model and Neural Networks. *International Journal of innovative Computing, Information and Control,* 7(6) 3545-3557.

Ciobotaru C, K. (2011), Load Forecasting for Remote Area Power Supply Systems. *Murdoch University School of Mathematical and Physical Sciences, Murdoch, Perth, W.A. 6150 and Power Electronics Research Unit, Curtin University, Bentley, Perth, W.A,* 6102, 231-237.

Chen, H. C., Chen, P. H., Cheng, L.Y., & Bai, W. X. (2013). Stand Alone Hybrid Generation System Based on Renewable Energy. *International Journal of Environmental Science and Development,* (IJES) DOI: 10.7763 4(5) 514-520.

Dan, S. (2008), Clarke's and Park's Transformations. *College of Electrical Engineering, Zhejiang University,* BPRA047, BPRA048, 1-47

Debosmita, D., Reza, E., & Dave, N. (2005). An Optimal Design of a Grid Connected Hybrid Wind/Photovoltaic/Fuel cell System for Distributed Energy Production. *Department of Electrical and Computer Engineering, the Ohio State University Columbus, USA.*

Deepak, K. L., Bibhuti, B., & Akella, A. K. (2011). Optimization of PV/Wind/Micro-Hydro/Diesel Hybrid Power System in HOMER for the Study Area. *International Journal on Electrical Engineering and Informatics*,3(3) 2011, 307-325.

Dimitris, I., Spyros, V., Panos, S., Fotis, S., & Costas, E. (2007). Power Management Strategies for aStand Alone Power System Using Renewable Energy Sources and Hydrogen Storage. *International Journal of Hydrogen Energy*, 34 7081-7095.

Dorin, B., Cristain, D. D., Arrian, G., & Adrian-Vasile, D. (2009). Isolated Hybrid Solar-Wind-Hydro Renewable Energy Systems. *Petrumaior, University of Tg. Mures, Electrical Engineering Department Romania*, 1-21.

Dorin, B., Cristian, D. D., Adrian, G., & Adrian-Vasile, D. (2012). Isolated Hybrid Solar-Wind-Hydro Renewable Energy Systems. *PetruMaior University of Tg. Mures, ElectricalEngineering Department Romania* 1-7.

Dumitru, C. D., Gligor, A., & Duka, A. V. (2009). Interdisciolinary in Engineering International Conference, PetruMaior. *University of TirgiMures, Romania,* 144-149.

Fei, D., Peng, L.,Bibin, H., Fei, G.,Chengdi, D., & Chenngshan, W. (2010). Modelling and Simu-lation of Grid Connected Hybrid Photovoltaic/Battery Distributed Generation System. *Key Laboratory of Power System Simulation and Control of Ministry of Education, Tianjin University, China,* 1-10.

Felix, A. F., & Godoy, M. S. (2006). Integration of Alternative Sources of Energy.*IEEE Press Wiley – Interscience, A John Wiley and Sons, INC Publication Copyright,* 1-23.

Graupe, D. (1997). Principle of Artificial Neural Networks, Advanced source on circuits and Systems. *World Scientific Publishing Co. Pte, Inc,* 1-303.

Meshram, S., Agnihotri, G., & Gupta, S. (2013). Performance Analysis of Grid Integrated Hydro and Solar Based Hybrid Systems. *Hindawi Publishing Corporation Advances in Power Electronics.* ID 697049, 1-7

Halimeh, R., Saeed, N., & Jamshid, K. (2012). Optimal sizing Method of Solar-Hydrogen Hybrid Energy System for Stand- alone Application Using Fuzzy Based Particle Swarm Optimization Algorithm. *Australian Journal of Basic and Applied Sciences,* 249-256.

Hussein, A., & Kamel, R. (2011). Shannon Entropy and Mean Square Error for Speeding the Convergence of Multilayer Neural Networks, a Comparative Approach. *Egyptian Informatics Journal, Cairo University*, 12, 197-209.

Hoque, M. M., Bhuiyan, I. K. A., Rajib, A., Farooque, A. A., & Aditya, S. K. (2012). Design analysis and performance study of a Hybrid PV- Diesel-Wind System for a Village Gopal Nagarin Comilla. *Global Journal of Science Frontier Research Physics and Space Science,* 12 (5) 11-19.

Hassan, A. S., Stephen, C., & James, R. (2013). Modelling of a Renewable Energy Powered Hydrogen Storage System at Baglan Hydrogen Centre. *Proceedings of the 11th International Conference on Fuel Cell Science, Engineering and Technology,* 1-9.

Isaac, A. S., Felly-Njoku, C. F., Aewale, A., & Ayokunle, A. A. (2014). Medium Term Load Forecasting of Covenant University Using the Regression Analysis Methods. *Journal of Energy Technology and Policy,* ISSN 2225-0573, 4(4) 10-17

Jianjun, W., Dongxiao, N., & Li, L. (2010). Middle-Long Term Load Forecasting Based on Dynamic Architecture for Artificial Neural Network. *Journal of Information & Computational Science* 7(8), 1711–1717.

Jimoh, B., Ogoh, W., & Muazu, M. B. (2007). Hybrid of solar and Small Hydro Electric Power System for Off-Grid Consumers. *Journal of Engineering and Technology, Moscow*, 23(5), 60-65.

Kaduna Sub-Transmission Network (2012), *Catalog on Planning and Construction PHCN*

Kaura, V. (1997). Operation of a Phase looked Loop System Under Distorted. *Journal of the Institute of Engineering Technology.* 1-33

Kaura, V. & Blasco, T, (1997). Optimal Operation of a Phase looked Loop System Under Distorted. *Journal of the Institute of Engineering Technology.* 1-33

Levine, K. Y.,& William, Y. T. (1999). Short-Term Load Forecasting Using an Artificial Neural Network. *Transactions on Power Systems* 7(1)8945-8950

Mahmet, K., & Ummuhan, B. F. (2009). Next Day Load Forecasting using Artificial Neural Network Models with Autoregression and Weighted Frequency Bin Blocks. *International Journal of Innovative Computing, Information and Control,* ISSN 1349-4198, 5, 889-898.

Marquez, J. L., Molina, M. G., & Pacas, J. M. (2009). Modelling and Simulation of Micro-Hydro Power Plants for Applications in Distributed Generation. *Tercer Congreso Nacional-Segundo Congreso Iberoamericano Hidrogeno y Fuentes Sustenables de Energia-* HYFUSEN 13-64

Meshram, S., Agnihotri, G., & Gupta, S. (2013). Modeling of Grid Connected DC Linked PV/Hydro Hybrid System. Electrical and Electronics Engineering: An International Journal (ELELIJ) Vol 2, No 3, 1-15

Naveen, R. J. (2013). Short Term Electric Load Prediction Using Artificial Neural Network. *International Journal of Engineering Research & Technology (IJERT)* ISSN: 2278-0181, 2 (7)2168-2172.

Ngo, G. (2010). Grid Converters for Photovoltaic and Wind Power Systems. *Applied Optics* 26, 4979-4984.

Ogren A, (2011). Harnessing Wind Energy to Solve Nigeria's Energy Crises. *The Pacific Journal of Science and Technology*, 10(2) 544-552.

Otun, J. A., Onemano, J. I., & Alayande, A. W. (2012). Assessment of the Hydropower Potential Of Kangimi Reservoir in Kaduna State Nigeria. *Nigerian Journal of Technology (NIJOTE-CH),*Vol.31, No. 3, pp. 300-307.

Puppala, S., & Ebraheem, M. (2012). Non-Conventional Power Generation Using Solar and Wind with the Aid of Hydro Power Generation. *International Journal of Engineering Research and Application (IJERA),* ISSN: 2248-9622 2(4) 271-274.

Rolim, D. R. (2006). Analysis and Software Implementation of a Robust Synchronizing PLL Circuit Based on the pq Theory. 53 (15). 191

Saeed, M. B.,& Ossama, B. A. (2013). Forecasting Electrical Load using ANN Combined with Fuzzy logic approach for forecasting half hourly Malaysia electricity load demand. *University Technology Malaysia Johor Darul Ta'zim*, 231-2317.

Samsher, K. S., & Unde, M. G. (2012). Short -Term Load Forecasting using Artificial Neural Network Technique. *International Journal of Engineering Sciences & Emerging Technologies,* 1(2), 97-107.

Teodorescu, R., Liserre, M., & Rodriguez, P. (2011). Grid Converters for Photovoltaic and Wind Power Systems. *Liserre, Politecnico di Bari, Itali, Riguez Technical University of Catalonia, Spain.* 1-175

Tiwari, S., Naresh, R., & Jha, R. (2013). Comparative Study of Back Propagation Algorithm in Neural Network Based Identification of Power System. *International Journal of Computer Science and Information technology,* IJCSIT, 5(4) 93-107.

Wang, W., & Song, C. (2014). Bayesian Regularization Neural Networks for Prediction of Silicon Content in Blast Furnance. *International Journal of advancements in computing Technology*,IJACT967PPL, 4(11) 336-343

Zehra, U., & Muhsin, T. G. (2013). Design and Simulation of a Solar Hydrogen System for Different Situations. *Cuarto Congreso Nacional-Tercer Congrsolbereomericano Hydrogenoy-fuentes Sustentables de Energgia HYFUSEN, Department of Electrical and Electronics En-gineering, Faculty of Engineering, Firat University,* 23119 Turkey 1-6.

APPENDIX A

Load Forecast Programme Based on Bayesian Regularization Algorithm

```
Close all, clear all, clc

% Importing Data

S = load ('magdata');
x = cons2seq (S.u);
t = const2seq (S.y);
% Network Architecture
hiddenLayerSize = 200;
net = fitnet(hiddenLayerSize);
net.input.processFcns = {'removeconstantrows','mapminmax'};       % Choosing
Input Pre/Post-Processing Functions
net.output.processFcns = {'removeconstantrows','mapminmax'};      % Choosing
Output Pre/Post-Processing Functions
net.divideFcn = 'dividerand';                          % Divide data randomly
net.divideMode = 'sample';                        % Divide up every sample
net.divideParam.trainRatio = 70/100;              % 70% Data for Training
net.divideParam.valRatio = 15/100;                % 15% Data for Validation
net.divideParam.testRatio = 15/100;               % 15% Data for Testing
% Training the Network
net.trainFcn = 'trainbr';                         % Train using Bayesian
Regularization
net.performFcn = 'sse';                   % Sum of squared error was used as
Performance Function
net.trainParam.epochs = 100;
[net,tr] = train(net,x,t);                        % perform Levenberg-Marquardt
training wiyh Bayesian regularization
y = net(x)                                % simulating the network over
complete input range
e = gsubtract(t,y)
performance = perform(net,t,y)
trainTargets = t .* tr.trainMask{1};                   % Recalculate Training
Performance
valTargets = t  .* tr.valMask{1};                 % Recalculate Validation
Performance
```

```
testTargets = t  .* tr.testMask{1};                    % Recalculate Training
Test Performance
trainPerformance = perform(net,trainTargets,y)  % Recalculate Training
Performance
valPerformance = perform(net,valTargets,y)             % Recalculate
Validation Performance
testPerformance = perform(net,testTargets,y)    % Recalculate Training Test
Performance
% View Network
view(net)                                    % View the Network
if (false)
genFunction(net,'myNeuralNetworkFunction');     % Examine the calculations
your trained neural network performs.
  y = myNeuralNetworkFunction(x);
% Generating Plots
net.plotFcns = {'plotperform','plottrainstate','ploterrhist',
'plotregression', 'plotfit'};    % Plot Functions
end
```

APPENDIX B

Data Obtained from Transmission Company of Nigeria and National Meteorological Agency

Months	Load Demand (MW)	Temperature (^oC)	Relative Humidity (%)	Rain fall (mm)	Wind speed (Km/s)	Solar radiation (w/m^2)	Sunshine (hours)
August 2010	17.55	24.0	83	327.8	59.48	582.3	4.9
September 2010	17.33	24.8	21.5	313.3	49.58	763.4	5.94
October 2010	18.31	24.9	77	149.3	47.90	729.37	7.2
November 2010	18.6	25.2	49	0	53.54	628	10.0
December 2010	18.53	26.6	30	0	70.77	645.8	9.5
January 2011	19.64	22.4	22	0	96.12	627.5	7.3
February 2011	20.22	27.6	29	1.3	56.92	635	7.6
March 2011	20.28	29.3	22	0	73.63	663	7.7
April 2011	20.82	29.2	40	57.1	62.14	708	6.9
May 2011	17.38	26.7	73	137.4	60.57	594	6.3
June 2011	16.77	25.5	76	80.9	60.27	557.8	4.9
July 2011	17.26	24.6	78	240.3	57.37	490.4	5.12
August 2011	16.08	23.4	82	208.0	52.99	543	4.9
September 2011	15.97	24.3	80	298.7	41.72	545	6.1
October 2011	16.30	25.0	73	72.7	31.92	727.4	5.9
November 2011	16.79	23.4	37	0	52.49	682	9.4
December 2011	17.54	22.3	26	0	78.47	654.3	8.2
January 2012	19.25	22.9	24	0	79.04	628.7	7.9
February 2012	19.46	27.4	22	0	60.16	643.9	6.3
March 2012	17.25	28.1	19	0	89.33	653.3	6.3
April 2012	18.37	28.7	58	61.6	69.76	763.8	6.8
May 2012	17.11	26.4	70	212.8	69.13	589.7	6.2
June 2012	24.08	25.3	76	100.3	61.08	762.39	4.7
July 2012	19.54	24.0	78	225.6	60.12	668.26	4.5
August 2012	17.59	23.5	83	346.2	52.33	533.21	4.0
September 2012	15.62	23.9	80	403.3	25.03	738.23	5.4
October 2012	16.88	25.5	75	135.1	11.28	792.02	7.3
November 2012	16.09	25.5	46	0	21.21	634.4	8.9
December 2012	18.63	23.9	30	0	49.79	635.2	9.1
January 2013	18.07	24.4	30	0	60.00	629.3	7.9
February 2013	16.45	26.8	30	0	57.01	639.2	7.3
March 2013	15.92	29.4	40	48.0	45.01	656.9	7.5
April 2013	16.13	28.4	60	74.3	56.41	683.8	6.9
May 2013	15.70	27.0	71	117.6	68.61	683.0	7.3
June 2013	15.25	25.3	76	286.5	69.39	762.39	4.8
July 2013	15.12	24.3	78.6	318.8	60.49	650.06	4.9

APPENDIX C

Data Obtained from National Meteorological Agency (NIMET) and Kaduna State Water Board

Months	Solar radiation	Discharge

	(w/m^2)	**(m^3/s) at H=6.04m**
August 2010	582.3	29.8
September 2010	763.4	33.2
October 2010	729.37	28.8
November 2010	628	25.3
December 2010	645.8	12.2
January 2011	627.5	22.8
February 2011	635	19.4
March 2011	663	20.6
April 2011	708	24.7
May 2011	594	27.5
June 2011	557.8	28.9
July 2011	490.4	33.4
August 2011	543	32.1
September 2011	545	30.2
October 2011	727.4	26.5
November 2011	682	25.9
December 2011	654.3	24.6
January 2012	628.7	21.4
February 2012	643.9	18.7
March 2012	653.3	19.3
April 2012	763.8	18.4
May 2012	589.7	26.9
June 2012	762.39	25.4
July 2012	668.26	27.4
August 2012	533.21	28.5
September 2012	738.23	34.2
October 2012	792.02	32.4
November 2012	634.4	28.2
December 2012	635.2	22.4
January 2013	629.3	19.8
February 2013	639.2	18.7
March 2013	656.9	22.5
April 2013	683.8	20.8
May 2013	683.0	27.8
June 2013	762.39	30.5
July 2013	650.06	32.4